International Journal of Physical Sciences

Volume 10 Number 11 16 June, 2015

ISSN 1992-1950

Academic Journals

ABOUT IJPS

The **International Journal of Physical Sciences (IJPS)** is published weekly (one volume per year) by Academic Journals.

International Journal of Physical Sciences (IJPS) is an open access journal that publishes high-quality solicited and unsolicited articles, in English, in all Physics and chemistry including artificial intelligence, neural processing, nuclear and particle physics, geophysics, physics in medicine and biology, plasma physics, semiconductor science and technology, wireless and optical communications, materials science, energy and fuels, environmental science and technology, combinatorial chemistry, natural products, molecular therapeutics, geochemistry, cement and concrete research, metallurgy, crystallography and computer-aided materials design. All articles published in IJPS are peer-reviewed.

Contact Us

Editorial Office: ijps@academicjournals.org

Help Desk: helpdesk@academicjournals.org

Website: http://www.academicjournals.org/journal/IJPS

Submit manuscript online http://ms.academicjournals.me/

Editorial Board

International Journal of Physical Sciences

Table of Contents: Volume 10 Number 11, 16 June, 2015

ARTICLES

academicJournals

Vol. 10(11), pp. 342-350, 16 June, 2015
DOI: 10.5897/IJPS2015.4287
Article Number: D9E8D2E53645
ISSN 1992 - 1950

http://www.academicjournals.org/IJPS

International Journal of Physical Sciences

Full Length Research Paper

Variational homotopy perturbation method for solving the generalized time-space fractional Schrödinger equation

A. M. S. Mahdy[1], A. S. Mohamed[1] and A. A. H. Mtawa[2]*

[1]Department of Mathematics, Faculty of Science, Zagazig University, Zagazig, Egypt.
[2]Department of Mathematics, Faculty of Science, Benghize University, Almarj, Libya.

Received 18 February, 2015; Accepted 26 May, 2015

We suggest and analyze a technique by combining the variational iteration method and the homotopy perturbation method. This method is called the variational homotopy perturbation method. We use this method for solving Generalized Time-space Fractional Schrödinger equation. The fractional derivative is described in Caputo sense. The proposed scheme finds the solution without any discritization, transformation or restrictive assumptions. Several example is given to check the reliability and efficiency of the proposed technique.

Key words: Caputo derivative, variational iteration method, homotopy perturbation method, Schrödinger equation.

INTRODUCTION

In recent years, considerable interest in fractional differential equations has been stimulated due to their numerous applications in the areas of nonlinear science (Dalir and Bashour, 2010), many important phenomena (Podlubny, 1999), engineering and physics (Miller and Ross, 1993), dielectric polarization (Sun et al., 1984), quantitative finance (Laskin, 2000).

To find explicit solutions of linear and nonlinear fractional differential equations, many powerful methods have been used such as the homotopy perturbation method (Momani and Odibat, 2007; Wang, 2008; Gupta and Singh, 2011), the Adomain decomposition method (Ray, 2009; Herzallah and Gepreel, 2012; Rida et al., 2008), the variational iteration method (He, 2000, 2004, 2007; He and Wang, 2007), the homotopy analysis method (Hemida et al., 2012; Gepreel and Mohamed, 2013; Ganjiani, 2010; Behzadi, 2011), the fractional complex transform (Ghazanfari, 2012; Su et al., 2013), the homotopy perturbation Sumudu transform method (Karbalaie et al., 2014; Mahdy et al., 2015), the local fractional variation iteration method (Yang and Baleanu, 2013; He and Liu, 2013; Yang et al., 2014), the local fractional Adomain decomposition method (Yang et al., 2013b), the Cantor-type Cylindrical-Coordinate method (Yang et al., 2013c), the variational iteration method with Yang-Laplace (Liu et al., 2013), the Yang-Fourier transform (Yang et al., 2013a), the Yang-Laplace transform (Zhao et al., 2014; Zhang et al., 2014) and variational homotopy perturbation method by (Noor and Mohyud-Din,2008). The variational homotopy perturbation

*Corresponding author. E-mail:hussanahmad65@yahoo.com

method (VHPM) is a combination of the variational iteration method and homotopy perturbation method. The suggested VHPM provides the solution in a rapid convergent series which may lead the solution in a closed form and is in full agreement with Rida et al. (2008), where similar problems were solved by using the decomposition method. The fact that the proposed technique solves nonlinear problems without using the so-called Adomian's polynomials is a clear advantage of this algorithm over the decomposition method.

In this paper, we investigate the application of the VHPM for solving the generalized time-space fractional Schrödinger equation with variable coefficients (Rida et al., 2008; Ganjiani, 2010):

$$i\frac{\partial^{\alpha}u}{\partial t^{\alpha}}+a\frac{\partial^{2\beta}u}{\partial t^{2\beta}}+v(x)u+\gamma|u|^{2}u=0, \tag{1}$$

Where $t>0$, $0<\alpha,\beta\leq 1$ with initial conditions

$$u(x,0)=u_{0}(x,t), \tag{2}$$

Where $u=u(x,t)$ is unknown function, $v(x)$ is the trapping potential, $0<\alpha,\beta\leq 1$ are parameters describing the order of the fractional Jumaries derivatives (Jumaries, 2007) and a,γ are a real constants, respectively. If we select $\alpha=\beta=1, v(x)=0,$ this equation turns to the famous nonlinear Schrödinger equation in optical fiber (Hao et al., 2004; Chen and Li, 2008; Li and Chen, 2004). In this paper, notice that Equation (1) is a complex differential equation with complex modulus term $|u|^{2}$, as we all know, a complex function $u(\zeta)$ can be written as $u(\zeta)\,e^{i\theta(\zeta)}$, where $c(\zeta)$ and $\theta(\zeta)$ are real functions, noticed that $|u(\zeta)|^{2}=|c(\zeta)|^{2}$, assume that $\lim_{n\to\infty}|\breve{u}|^{2}=|u|^{2}=|u_{0}|^{2}$, we get the VHPM for Equation (1).

BASIC DEFINITIONS OF FRACTIONAL CALCULUS

Here, we present the basic definitions and properties of the fractional calculus theory, which are used further in this paper.

Definition 1

A real function $f(t), t>0,$ f(t), is said to be in the space $C_{\sigma}, \sigma\in R$, if there exists a real number $p>\sigma$ such that $f(t)=t^{p}f_{1}(t)$ where $f_{1}(t)\in[0,\infty)$, and it is said to be in the space C_{σ}^{m} if $f^{m}\in C_{\sigma},\ m\in\mathrm{N}$.

Definition 2

The left sided Riemann-Liouville fractional integral of order $\alpha\geq 0$, of a function $f\in C_{\sigma},\sigma\geq -1$ is defined as:

$$J^{\alpha}f(t)=\frac{1}{\Gamma(\alpha)}\int_{0}^{t}(t-\zeta)^{\alpha-1}f(\zeta)\,d\zeta \tag{3}$$

where $\alpha>0, t>0$ and $\Gamma(\alpha)$ is the Gamma function. Also one has the following properties:

$$\begin{aligned}&J^{\alpha}J^{\beta}f(x)=J^{\alpha+\beta}f(x),\\&J^{\alpha}J^{\beta}f(x)=J^{\beta}J^{\alpha}f(x),\\&J^{\alpha}x^{\gamma}=\frac{\Gamma(\gamma+1)}{\Gamma(\alpha+\gamma+1)}x^{\alpha+\gamma}.\end{aligned} \tag{4}$$

Definition 3

Let $f\in C_{m}^{n}, n\in\mathrm{N}\cup\{0\}$. The left sided Caputo fractional derivative of f in the Caputo sense is defined by Podlubny (1999) and He (2014) as follows:

$$D_{t}^{\alpha}f(t)=\begin{cases}\dfrac{1}{\Gamma(n-\alpha)}\displaystyle\int_{0}^{t}(t-\zeta)^{n-\alpha-1}f^{(n)}(\zeta)\ d(\zeta), & n-1<\alpha\leq n,\\ D_{t}^{\alpha}f(t), & \alpha=n,\end{cases} \tag{5}$$

Also one has the following properties:

$$\begin{aligned}&D^{\alpha}C=0,\quad (C \text{ is constant }),\\&D^{\alpha}x^{\gamma}=\begin{cases}\dfrac{\Gamma(\gamma+1)}{\Gamma(\gamma-\alpha+1)}x^{\gamma-\alpha}, & \gamma>\alpha-1,\\ 0, & \gamma\leq\alpha-1,\end{cases}\\&J^{\alpha}D^{\alpha}f(x)=f(x)-\sum_{k=0}^{n-1}f^{(k)}(0^{+})\frac{x^{k}}{k!},\quad n-1<\alpha\leq n,\\&D^{\alpha}J^{\alpha}f(x)=f(x).\end{aligned} \tag{6}$$

Definition 4

The single parameter and the two parameters variants of the Mittag-Leffler function are denoted by $E_{\alpha}(t)$ and $E_{\alpha,\beta}(t)$, respectively, which are relevant for their connection with fractional calculus, and are defined as:

$$E_{\alpha}(t)=\sum_{j=0}^{\infty}\frac{t^{j}}{\Gamma(\alpha j+1)}, \quad \alpha>0, \quad t\in C, \tag{7}$$

$$E_{\alpha,\beta}(t)=\sum_{j=0}^{\infty}\frac{t^{j}}{\Gamma(\alpha j+\beta)}, \quad \alpha,\beta>0, \quad t\in C. \tag{8}$$

Some special cases of the Mittag-Leffler function are as follows:

$$E_1(t)=e^t,$$
$$E_{\alpha,1}(t)=E_{\alpha}(t).$$

Other properties of the Mittag-Leffler functions can be found in Kilbas et al. (2004). These functions are generalizations of the exponential function, because, most linear differential equations of fractional order have solutions that are expressed in terms of these functions.

VARIATIONAL ITERATION METHOD

To illustrate the basic concept of the technique, we consider the following general differential equation:

$$L(u)+N(u)-f(x)=0, \tag{9}$$

where L is a linear operator, N a nonlinear operator, and $f(x)$ the function term. In the variational iteration method (He, 2000, 2004, 2007; He and Wang, 2007), a correction functional can be constructed as follows:

$$u_{n+1}(x)=u_n(x)+\int_0^x \lambda(Lu_n(s)+N\breve{u}_n(s)-f(s))\,ds, \tag{10}$$

Where λ is a general Lagrange multiplier (He, 2000, 2004, 2007; He and Wang, 2007) , which can be identifed optimally via a variational iteration method. The subscripts n denote the nth approximation, $\breve{u}_n$ is considered as a restricted variation. That is, $\delta\breve{u}_n=0$; equation (10) is called a correct functional. The solution of the linear problems can be solved in a single iteration step due to the exact identification of the Lagrange multiplier. The principles of the variational iteration method and its applicability for various kinds of differential equations are given in (He, 2000, 2004, 2007; He and Wang, 2007). With λ determined then several approximation u_{n+1}, $n\geq 0$ follow immediately. Consequently, the exact solution may be obtained by using $u=\lim_{n\to\infty}u_n$.

HOMOTOPY PERTURBATION METHOD

Consider the following nonlinear differential equation

$$A(u)-f(x)=0, \quad x\in\Omega, \tag{11}$$

Subject to the conditions

$$B(u,\partial u/\partial m)=0, \quad x\in\Gamma, \tag{12}$$

Where A is a general differential operator, B is a boundary operator, $f(x)$ is a known an analytical function, Γ is boundary of the domain Ω and $\partial/\partial m$ denotes directional derivative.

The operator A can be decomposed into a linear operator, denoted by L, and a nonlinear operator, denoted by N. Therefore, Equation (11) can be written as follows:

$$L(u)+N(u)-f(x)=0. \tag{13}$$

By the homotopy technique we construct defined as $v(x,p):\Omega\times[0,1]\to R$ with satisfies:

$$H(v,p)=(1-p)[L(v)-L(u_0)]+p[A(u)-f(x)]=0, \quad 0\leq p\leq 1, \tag{14}$$

Which is equivalent to

$$H(v,p)=L(v)-L(u_0)+pL(u_0)+p[N(u)-f(x)]=0, \quad 0\leq p\leq 1, \tag{15}$$

Where u_0 is the initial approximation of Equation (11) that satisfies the boundary condition and p is an embedding parameter.

When the value of p is changed from zero to unity, we can easily see that

$$H(v,0)=L(v)-L(u_0)=0, \tag{16}$$

$$H(v,1)=L(v)-N(v)-f(x)=A(u)-f(x)=0, \tag{17}$$

in topology, this changing process is called deformation, and Equations (16) and (17) are called homotopic. If the p-parameter is considered as small, then the solution of Equations (13) and (14) can be expressed as a power series in p as follows:

$$v=v_0+pv_1+p^2v_2+p^3v_3+\cdots \tag{18}$$

The best approximation for the solution of Equation (11) is

$$u=\lim_{p\to 1}v=v_0+v_1+v_2+v_3+\cdots \tag{19}$$

It is well known that series (18) is convergent for most of the cases and also the rate of convergence is dependent on $L(u)$; (Momani and Odibat, 2007; Wang, 2008; Gupta and Singh, 2011). We assume that Equation (19) has a unique solution. The comparisons of like powers of p give solutions of various orders.

VARIATIONAL HOMOTOPY PERTURBATION METHOD (VHPM)

To convey the basic idea of the variational homotopy perturbation method, we consider the following general differential equation:

$$Lu + Nu = f(x), \tag{20}$$

Where L is the linear operator, N is the general nonlinear operator and $f(x)$ the forcing term. According to variational iteration method (He, 2000, 2004, 2007; He and Wang, 2007), we can construct a correct functional as follows:

$$u_{n+1}(x) = u_n(x) + \int_0^x \lambda(\zeta)(Lu_n(\zeta) + N\breve{u}_n(\zeta) - f(\zeta))\, d\zeta, \tag{21}$$

Where λ is a Lagrange multiplier (He, 2000, 2004, 2007; He and Wang, 2007), which can be identified optimally via variational iteration method. The subscripts n denote the nth approximation, $\breve{u}_n$ is considered as a restricted varation. That is, $\delta\, \breve{u}_n = 0$; Equation (21) is called as a correct functional. Now, we apply the homotopy perturbation method.

$$\sum_{n=0}^{\infty} p^{(n)} u_n = u_0(x) + \int_0^x \lambda(\zeta)\left(\sum_{n=0}^{\infty} p^{(n)} L(u_n) + \sum_{n=0}^{\infty} p^{(n)} N(\breve{u}_n) - f(\zeta)\right) d\zeta, \tag{22}$$

Which is the variational homotopy perturbation method and is formulated by the coupling of variational iteration method and Adomian's polynomials. A comparison of like powers of p gives solutions of various orders.

APPLICATIONS

Here, we apply the VHPM developed in Section 5 for solving the Generalized Time-space Fractional Schrödinger Equation with variable coefficients. We develop the correct functional and calculate the Lagrange multipliers optimally via variational theory. The homotopy perturbation method is implemented on the correct functional and finally, comparison of like powers of p gives solutions of various orders. Numerical results reveal that the VHPM is easy to implement and reduces the computational work to a tangible level while still maintaining a very higher level of accuracy. For the sake of comparison, we take the same examples as used in (Herzallah and Gepreel, 2012; Rida et al., 2008; Wazwaz, 2008; Hong and Lu, 2014).

Example 1

We first consider the time-fractional NLS equation:

$$i\frac{\partial^\alpha u}{\partial t^\alpha} + a\frac{\partial^2 u}{\partial x^2} + \gamma|u|^2 u = 0, \tag{23}$$

where $t > 0$, $0 < \alpha, \beta \le 1$ with initial conditions

$$u(x,0) = A\sec h(x), \tag{24}$$

The correct functional is given as:

$$u_{n+1}(x,t) = A\sec h(x) + \int_0^x \lambda(\zeta)\left(\frac{\partial^\alpha u_n}{\partial t^\alpha} - ia\frac{\partial^2 \breve{u}_n}{\partial t^2} - i\gamma\breve{u}_n|u_0|^2\right) d\zeta, \tag{25}$$

Where $\breve{u}_n$ is considered as restricted variation. Making the above functional stationary, the Lagrange multiplier can be determined as $\lambda = -1$, which yields the following iteration formula:

$$u_{n+1}(x,t) = A\sec h(x) - J^\alpha\left[\frac{\partial^\alpha u_n}{\partial t^\alpha} - ia\frac{\partial^2 \breve{u}_n}{\partial x^2} - i\gamma\breve{u}_n|u_0|^2\right]. \tag{26}$$

Applying the variational homotopy perturbation method, we have

$$u_0 + pu_1 + p^2u_2 + p^3u_3 + \cdots = A\sec h(x) - pJ^\alpha\begin{pmatrix}\left(\frac{\partial^\alpha u_0}{\partial t^\alpha} + p\frac{\partial^\alpha u_1}{\partial t^\alpha} + p^2\frac{\partial^\alpha u_2}{\partial t^\alpha} + \cdots\right) \\ -ia\left(\frac{\partial^2 \breve{u}_0}{\partial x^2} + p\frac{\partial^2 \breve{u}_1}{\partial x^2} + p^2\frac{\partial^2 \breve{u}_2}{\partial x^2} + \cdots\right) \\ -i\gamma\left(\breve{u}_0 + p\breve{u}_1 + p^2\breve{u}_2 + \cdots\right)|u_0|^2\end{pmatrix}, \tag{27}$$

Comparing the coefficient of like powers of p, we have

$$p^0 : u_0(x,t) = A\sec h(x),$$

$$p^1 : u_1(x,t) = A\left(\sec h(x) - 2\sec h^3(x)\right)\frac{ait^\alpha}{\Gamma(\alpha+1)} + i\gamma A^3 \sec h^3(x)\frac{t^\alpha}{\Gamma(\alpha+1)}$$

$$= A\sec h(x)\frac{ait^\alpha}{\Gamma(\alpha+1)}, \quad \left(A^2 = \frac{2a}{\gamma}\right),$$

$$p^2 : u_2(x,t) = A\left(\sec h(x) - 2\sec h^3(x)\right)\frac{(a\,it^\alpha)^2}{\Gamma(2\alpha+1)} + i\gamma A^3 \sec h^3(x)\frac{a(it^\alpha)^2}{\Gamma(2\alpha+1)}$$

$$= A\sec h(x)\frac{(a\,it^\alpha)^2}{\Gamma(2\alpha+1)},$$

$$p^3 : u_3(x,t) = A\sec h(x)\frac{(ait^\alpha)^3}{\Gamma(3\alpha+1)},$$

$$p^n : u_n(x,t) = A\sec h(x)\frac{(ait^\alpha)^n}{\Gamma(n\alpha+1)}. \tag{28}$$

Thus the solution of Equation (23) is given by

$$\begin{aligned} u(x,t) &= \lim_{p\to 0}\sum_{n=0}^{\infty} p^n u_n(x,t) \\ &= A\sec h(x)\left(1 + \frac{ait^\alpha}{\Gamma(\alpha+1)} + \frac{(ait)^2}{\Gamma(2\alpha+1)} + \frac{(ait)^3}{\Gamma(3\alpha+1)} + \cdots\right) \\ &= A\sec h(x)\sum_{n=0}^{\infty}\frac{(ait^\alpha)^n}{\Gamma(n\alpha+1)} \\ &= A\sec h(x)\, E_\alpha(ait^\alpha). \end{aligned} \tag{29}$$

If we put $\alpha \to 1$ in Equation (29) or solve Equations (23) and (24) with $\alpha = 1$, we obtain the exact solution

$$u(x,t) = A\operatorname{sec}h(x)\sum_{n=0}^{\infty}\frac{(ait^{\alpha})^n}{\Gamma(n\alpha+1)}$$
$$= \pm\sqrt{\frac{2a}{\gamma}}\operatorname{sec}h(x)\ e^{iat}.$$

Which is in full agreement with the result in Hong and Lu, (2014)

Example 2

We first consider the time-space fractional NLS equation:

$$i\frac{\partial^{\alpha}u}{\partial t^{\alpha}} + a\frac{\partial^{2\beta}u}{\partial x^{2\beta}} + 2a|u|^2 u = 0, \qquad (30)$$

Where $t > 0$, $0 < \alpha, \beta \le 1$ with initial conditions

$$u(x,0) = e^{ix}, \qquad (31)$$

The correct functional is given as

$$u_{n+1}(x,t) = e^{ix} + \int_0^x \lambda(\zeta)\left(\frac{\partial^{\alpha}u_n}{\partial t^{\alpha}} - ia\frac{\partial^{2\beta}\breve{u}_n}{\partial t^{2\beta}} - 2ia\gamma\breve{u}_n|u_0|^2\right)d\zeta, \quad (32)$$

Where $\breve{u}_n$ is considered as restricted variation. Making the above functional stationary, the Lagrange multiplier can be determined as $\lambda = -1$, which yields the following iteration formula:

$$u_{n+1}(x,t) = e^{ix} - J^{\alpha}\left[\frac{\partial^{\alpha}u_n}{\partial t^{\alpha}} - ia\frac{\partial^{2\beta}\breve{u}_n}{\partial x^{2\beta}} - 2ia\breve{u}_n|u_0|^2\right]. \quad (33)$$

Applying the variational homotopy perturbation method, we have:

$$u_0 + pu_1 + p^2u_2 + p^3u_3 + \cdots = e^{ix} - pJ^{\alpha}\begin{pmatrix}\left(\frac{\partial^{\alpha}u_0}{\partial t^{\alpha}} + p\frac{\partial^{\alpha}u_1}{\partial t^{\alpha}} + p^2\frac{\partial^{\alpha}u_2}{\partial t^{\alpha}} + \cdots\right)\\ -ia\left(\frac{\partial^{2\beta}\breve{u}_0}{\partial x^{2\beta}} + p\frac{\partial^{2\beta}\breve{u}_1}{\partial x^{2\beta}} + p^2\frac{\partial^{2\beta}\breve{u}_2}{\partial x^{2\beta}} + \cdots\right)\\ -2ia\left(\breve{u}_0 + p\breve{u}_1 + p^2\breve{u}_2 + \cdots\right)|u_0|^2\end{pmatrix}, \quad (34)$$

Comparing the coefficient of like powers of p, we have:

$$p^0 : u_0(x,t) = e^{ix},$$

$$p^1 : u_1(x,t) = \left[aie^{ix}e^{i\pi\beta} + 2aie^{ix}\right]\frac{at^{\alpha}}{\Gamma(\alpha+1)}$$
$$= e^{ix}\left(2 + e^{i\pi\beta}\right)\frac{ait^{\alpha}}{\Gamma(\alpha+1)},$$
$$p^2 : u_2(x,t) = \left[e^{ix}\left(2+e^{i\pi\beta}\right)e^{i\pi\beta} + 2e^{ix}(2+e^{i\pi\beta})\right]\frac{(ait^{\alpha})^2}{\Gamma(2\alpha+1)}$$
$$= e^{ix}(2+e^{i\pi\beta})^2\frac{(ait^{\alpha})^2}{\Gamma(2\alpha+1)},$$
$$p^3 : u_3(x,t) = e^{ix}(2+e^{i\pi\beta})^3\frac{(ait^{\alpha})^3}{\Gamma(3\alpha+1)},$$
$$p^n : u_n(x,t) = e^{ix}(2+e^{i\pi\beta})^n\frac{(ait^{\alpha})^n}{\Gamma(n\alpha+1)}. \qquad (35)$$

Thus the solution of Equation (30) is given by:

$$u(x,t) = \lim_{p\to 0}\sum_{n=0}^{\infty}p^n u_n(x,t)$$
$$= e^{ix}\left(1 + \frac{(2+e^{i\pi\beta})a\,it^{\alpha}}{\Gamma(\alpha+1)} + \frac{(2+e^{i\pi\beta})^2(a\,it)^2}{\Gamma(2\alpha+1)} + \frac{(2+e^{i\pi\beta})^3(a\,it)^3}{\Gamma(3\alpha+1)} + \cdots\right)$$
$$= e^{ix}\sum_{n=0}^{\infty}(2+e^{i\pi\beta})^n\frac{(a\,it^{\alpha})^n}{\Gamma(n\alpha+1)}$$
$$= e^{ix}E_{\alpha}(a\,i(2+e^{i\pi\beta})t^{\alpha}). \qquad (36)$$

If we put $\alpha \to 1$ in Equation (36) or solve Equations (30) and (31) with $\alpha = 1$, we obtain the exact solution

$$u(x,t) = e^{ix}\sum_{n=0}^{\infty}(2+e^{i\pi\beta})^n\frac{(ait^{\alpha})^n}{\Gamma(n\alpha+1)}$$
$$= e^{i(x+at)}.$$

Which is in full agreement with the result of Herzallah and Gepreel (2012); Wazwaz (2008) and Hong and Lu (2014).

Example 3

We first consider the time-space fractional NLS equation:

$$i\frac{\partial^{\alpha}u}{\partial t^{\alpha}} + \frac{1}{2}\frac{\partial^{2\beta}u}{\partial x^{2\beta}} - u\cos^2(x) - |u|^2 u = 0, \qquad (37)$$

Where $t > 0$, $0 < \alpha, \beta \le 1$ with initial conditions

$$u(x,0) = \sin(x), \qquad (38)$$

The correct functional is given as:

Table 1. Comparison between the real part of u_4 and u when $\alpha=\beta=1$.

x	t	**Approximate** u_{4appr}	**Exact solution**	**Absolute error**
0.2	0.1	0.1964384915	0.1964384884	3.1×10^{-9}
3	0.2	0.1348172358	0.1348170931	1.427×10^{-7}
15	0.3	0.5855572742	0.5855498014	7.4728×10^{-6}
5	0.4	-0.7914960966	-0.7914343559	6.17407×10^{-5}

$$u_{n+1}(x,t)=\sin(x)+\int_0^x \lambda(\zeta)\left(\frac{\partial^\alpha u_n}{\partial t^\alpha}-i\frac{1}{2}\frac{\partial^{2\beta}\breve{u}_n}{\partial t^{2\beta}}+i\breve{u}\cos^2(x)+i\breve{u}_n|u_0|^2\right)d\zeta, \quad (39)$$

Where $\breve{u}_n$ is considered as restricted variation. Making the above functional stationary, the Lagrange multiplier can be determined as $\lambda=-1$, which yields the following iteration formula:

$$u_{n+1}(x,t)=\sin(x)-J^\alpha\left[\frac{\partial^\alpha u_n}{\partial t^\alpha}-\frac{i}{2}\frac{\partial^2\breve{u}_n}{\partial x^2}+i\breve{u}\cos^2(x)+i\breve{u}_n|u_0|^2\right]. \quad (40)$$

Applying the variational homotopy perturbation method, we have

$$u_0+pu_1+p^2u_2+p^3u_3+\cdots=\sin(x)-pJ^\alpha\begin{pmatrix}\left(\frac{\partial^\alpha u_0}{\partial t^\alpha}+p\frac{\partial^\alpha u_1}{\partial t^\alpha}+p^2\frac{\partial^\alpha u_2}{\partial t^\alpha}+\cdots\right)\\ -\frac{i}{2}\left(\frac{\partial^{2\beta}\breve{u}_0}{\partial x^{2\beta}}+p\frac{\partial^{2\beta}\breve{u}_1}{\partial x^{2\beta}}+p^2\frac{\partial^{2\beta}\breve{u}_2}{\partial x^{2\beta}}+\cdots\right)\\ +i(\breve{u}_0+p\breve{u}_1+p^2\breve{u}_2+\cdots)\cos^2(x)\\ +i(\breve{u}_0+p\breve{u}_1+p^2\breve{u}_2+\cdots)|u_0|^2\end{pmatrix}, \quad (41)$$

Comparing the coefficient of like powers of p, we have

$$p^0: u_0(x,t)=\sin(x),$$

$$p^1: u_1(x,t)=\left[\frac{1}{2}\sin(x+\pi\beta)-\sin(x)\right]\frac{it^\alpha}{\Gamma(\alpha+1)}$$

$$p^2: u_2(x,t)=\left[\frac{1}{4}\sin(x+2\pi\beta)-\sin(x+\pi\beta)+\sin(x)\right]\frac{(it^\alpha)^2}{\Gamma(2\alpha+1)}$$

$$p^3: u_3(x,t)=\left[\frac{1}{8}\sin(x+3\pi\beta)-\frac{3}{4}\sin(x+2\pi\beta)+\frac{3}{2}\sin(x+\pi\beta)-\sin(x)\right]\frac{(it^\alpha)^3}{\Gamma(3\alpha+1)},$$

$$p^4: u_4(x,t)=\left[\frac{1}{16}\sin(x+4\pi\beta)-\frac{1}{2}\sin(x+3\pi\beta)+\frac{3}{2}\sin(x+2\pi\beta)-2\sin(x+\pi\beta)+\sin(x)\right]\frac{(it^\alpha)^4}{\Gamma(4\alpha+1)}, \vdots$$

$$p^n: u_n(x,t)=C_n(x)\frac{(it^\alpha)^n}{\Gamma(n\alpha+1)}, \quad (42)$$

Where

$$C_n(x)=C_{n,0}(x)\sin(x)+C_{n,1}(x)\sin(x+\pi\beta)+C_{n,2}(x)\sin(x+2\pi\beta)+\cdots+C_{n,n}(x)\sin(x+n\pi\beta)$$

And where

$$C_{n,0}=(-1)^n, \quad n\ge 0,$$

$$C_{n,1}=\frac{1}{2}C_{n-1,0}-C_{n-1,1}, \quad n>1,$$

$$C_{n,2}=\frac{1}{2}C_{n-1,1}-C_{n-1,2}, \quad n>2,$$

$$\vdots$$

$$C_{n,i+1}=\frac{1}{2}C_{n-1,i}-C_{n-1,i+1}, \quad i=0,1,2,\ldots$$

$$C_{n,n}=\frac{1}{2}C_{n-1,n-1}, \quad n\ge 1.$$

Thus the solution of Equation (37) is given by:

$$\begin{aligned}u(x,t)&=\lim_{p\to 0}\sum_{n=0}^{\infty}p^n u_n(x,t)\\ &=e^{ix}\sum_{n=0}^{\infty}C_n(x)\frac{(it^\alpha)^n}{\Gamma(n\alpha+1)}\\ &=\sin\left[\frac{x^\beta}{\Gamma(\beta+1)}\right]Exp\left[\frac{-3it^\alpha}{2\Gamma(\alpha+1)}\right].\end{aligned} \quad (43)$$

If we put $\alpha\to 1$ in Equation (43) or solve Equation (37) and (38) with $\alpha=1$, we obtain the exact solution

$$\begin{aligned}u(x,t)&=e^{ix}\sum_{n=0}^{\infty}C_n(x)\frac{(it^\alpha)^n}{\Gamma(n\alpha+1)}\\ &=\sin(x)e^{\left(-3/2\right)it}.\end{aligned}$$

Which is in full agreement with the result of Rida et al. (2008) and Hong and Lu (2014).

Comparisons between the real part of some numerical results and the exact solution (43) are summarized in Tables 1 and 2, and the simulations for u_4, u_{abs}, and u are plotted in Figures 1 and 2, which shows that VHPM produced a rapidly convergent series.

Comparisons between the imaginary part and the exact solution Equation (43) are plotted in Figures 3 and 4, and the simulations for u_5; $u_{abs}\upsilon$ and υ, which shows that VHPM produced a rapidly convergent series.

Table 2. Comparison between the real part of u_4 and u when $\alpha = 0.7,\ \beta = 0.9$.

x	t	**Approximate** u_{4appr}	**Exact solution**	**Absolute error**
0.2	0.1	0.1989280524	0.2288404399	0.0299123875
0.2	0.2	0.1978265247	0.2080382267	0.010211702
1	0.3	0.6273816436	0.6355277868	0.0081461432
2	0.4	0.5092408030	0.6018550035	0.0926142005

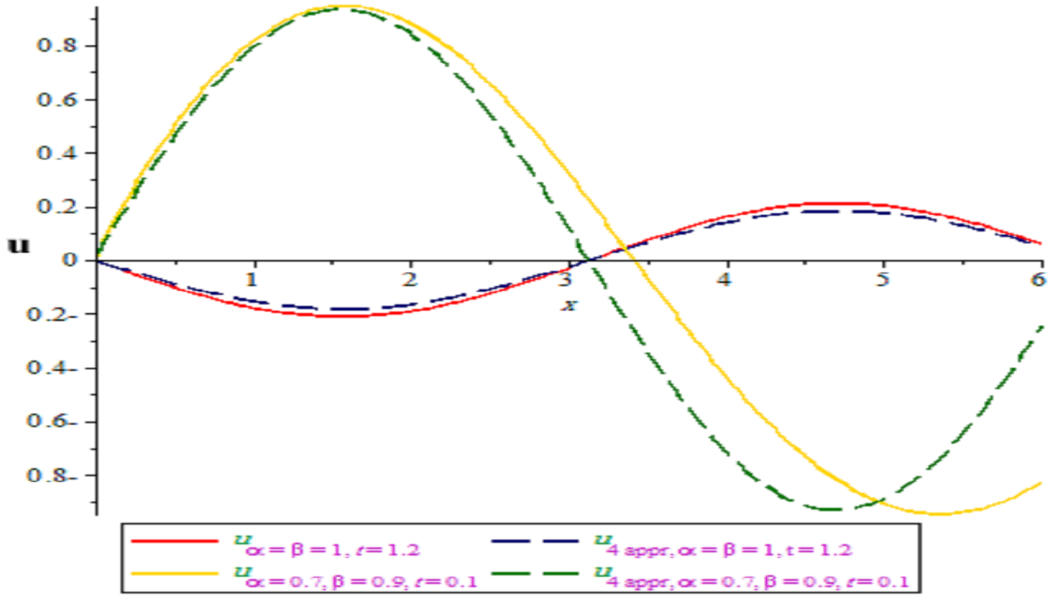

Figure 1. Comparison between the real part of u_4 and the exact solution υ .

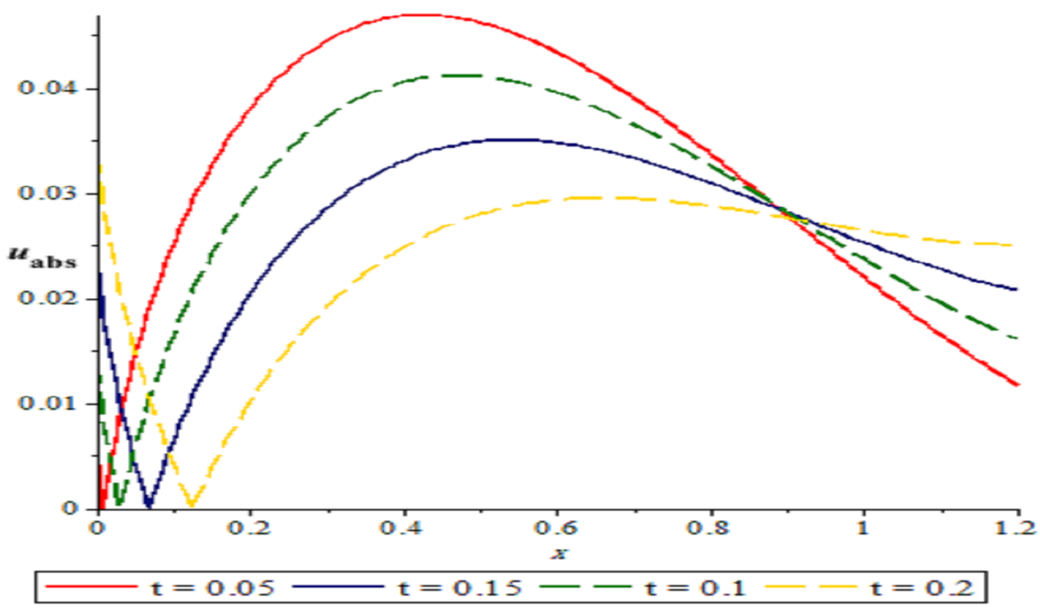

Figure 2. Plots of the absolute error u_{abs} when $\alpha = 0.7$ and $\beta = 0.9$.

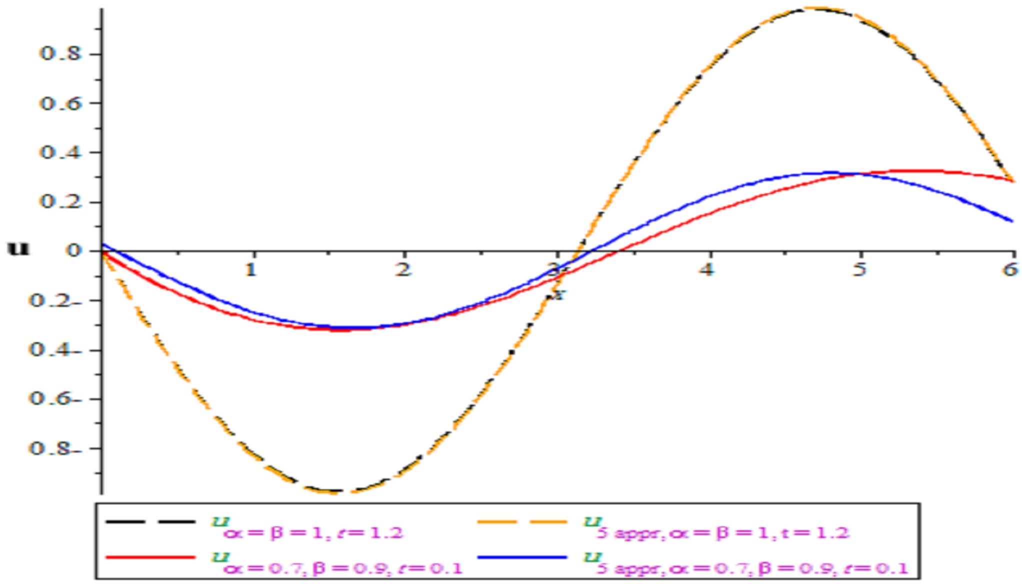

Figure 3. Comparison between the imaginary part of u_5 and the exact solution υ.

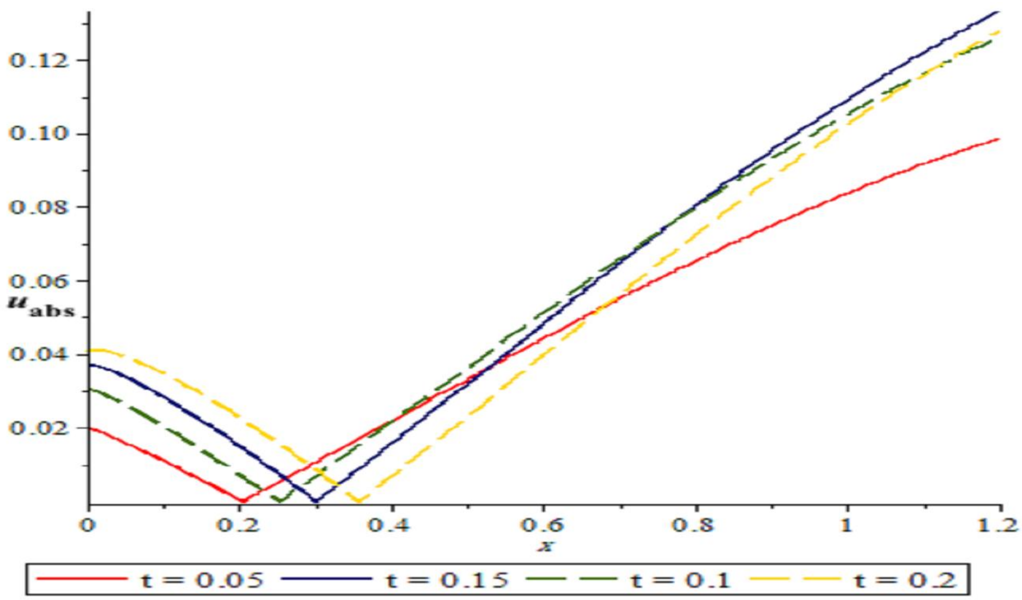

Figure 4. Plots of the absolute error u_{abs} when $\alpha = 0.7$ and $\beta = 0.9$.

CONCLUSIONS

In this paper, we have introduced a combination of the variational iteration method and homotopy perturbation method for time-space fractional equations. This combination builds a strong method called the VHPM. We used the variational homotopy perturbation method for solving the Generalized Time-space Fractional Schrödinger Equation with variable coefficient. The VHPM has been shown to solve effectively, easily and accurately a large class of nonlinear problems with the approximations which convergent are rapidly to exact solutions. The obtained results are compared well with those obtained by VIM, ADM, HAM, MFVIM. Finally, we conclude that the VHPM may be considered as a nice refinement in existing numerical techniques.

Conflict of Interest

The authors have not declared any conflict of interest.

ACKNOWLEDGEMENT

The authors wish to thank the referees for their comments.

REFERENCES

Behzadi SS (2011). Solving Schrödinger equation by using modified variational iteration and homotopy analysis methods. J. Appl. Anal. Comput. 1(4):427-437.

Chen Y, Li B (2008). An extended sub equation rational expansion method with symbolic compuation and solutions of the nonlinear Schrödinger equation model. Nonlinear Analysis: Hybrid Systems. 2(2):242-255.

Dalir M, Bashour M (2010). Applications of fractional calculus. Appl. Math. Sci. 4:1021-1032.

Ganjiani M (2010). Solution of nonlinear fractional differential equations using homotopy analysis method. Appl. Mathematical Model. Simul. Comput. Eng. Environ. Syst. 34(6):1634-1641.

Gepreel KA, Mohamed MS(2013). Analytical approximate solution for nonlinear space-time fractional Klein-Gordon equation. Chin. Phys. B. 22(1):010201-010211.

Ghazanfari B, Ghazanfari AG (2012). Solving fractional nonlinear Schrödinger equation by fractional complex transform method. Int. J. Math. Model. Comput. 2(4):277-281.

Gupta Pk, Singh M (2011). Homotopy perturbation method for fractional Fornberg-Whitham equation. Computers and Mathematics with Applications. 61(2):250-254.

Hao R, Li L, Li Z, Xue W, Zhou G (2004). A new approach to exact solition solutions and solition interaction for nonlinear Schrödinger equation with variable coefficients. Opt. Commun. 236(1-3):79-86.

He JH (2000). Variational iteration method for autonomous ordinary differential. Appl. Math. Comput. 114:115-123.

He JH (2004). Variational principle for some nonlinear partial differential equations with variable coefficients. Chaos Solitons Fractals. 19:847-851.

He JH (2007). Variational iteration method some recent results and new interpretations. J. Comp. Appl. Math. 367:188-191.

He JH (2014). A Tutorial Review on fractional space-time and fractional calculus. Int. J. Theoretical Phys. 53(11):3698-3718.

He JH, Liu FJ (2013). Local fractional variational iteration method for fractional heat transfer in silk cocoon hierarchy. Nonlinear Sci. Lett. A. 4(1):15-20.

He JH, Wang SQ (2007). Variational iteration method for solving integro-differential equations. Phys. Lett. A. 207:3-17.

Hemida KM, Gepreel KA, Mohamed MS (2012). Analytical approximate solution to the time-space nonlinear fractional differential equations. Int. J. Pure Appl. Math. 78(2):233-243.

Herzallah MAE, Gepreel KA (2012). Approximate solution to the time-space fractional cubicnonlinear Schrödinger equation. Appl. Math. Model. Simul. Comput. Eng. Environ. Syst. 36(11):5678-5685.

Hong B, Lu D (2014). Modified fractional variational iteration method for solving the generalized time-space fractional Schrödinger equation. Sci. World J. Article ID 964643, P. 6.

Jumarie G (2007). Fractional partial differential equations and modified Riemann-Liouville derivative new methods for solution. J. App. Math. Comput. 1:31-48.

Karbalaie A, Montazeri MM, Muhammed HH (2014). Exact solution of Time-Fractional partial differential equations using Sumudu transform. Wseast Trans. Math. 13:142-151.

Kilbas AA, Saigo M, Saxena RK (2004). Generalized Mittag-Leffler function and generalized fractional calculus operators. Integral Transforms Special Func. 15:31-49.

Laskin N (2000). Fractional market dynamics. Physica A. 287(3-4):482-492.

Li B, Chen Y (2004). On exact solutions of the nonlinear Schrödinger equations in optical fiber. Chaos Solitons Fractals 21(1):241-247.

Liu CF, Kong SS, Yuan SJ (2013). Reconstructive schemes for variational iteration method with in Yang-Laplace transform with application to fractional heat conduction problem. Thermal Sci. 117(3):715-721.

Mahdy AMS, Mohamed AS, Mtawa AAH (2105). Implementation of the homotopy perturbation Sumudu transform method for solving Klein-Gordon equation. Appl. Math. 6:617-628.

Miller KS, Ross B (1993). An Introduction to the Fractional Calculus and Fractional Differential Equations. John Wiley & Sons, New York, NY, USA.

Momani S, Odibat Z (2007). Homotopy perturbation method for nonlinear partial differential equations of fractional order. Physica Lett. A. 365(5-6):345-350.

Noor MA, Mohyud-Din ST (2008). Variational homotopy perturbation method for solving higher dimensional intial boundary value problems. Math. Problems Eng. Article ID 696734, P. 11.

Podlubny I (1999). Fractional Differential Equations. Academic Press, New York, NY, USA.

Ray SS (2009). Analytical solution for the space fractional diffusion equation by two-step Adomian decomposition method. Commun. Nonlinear Sci. Numer. Simul. 14(4):1295-1306.

Rida SZ, El-sherbiny HM, Arafa AAM (2008). On the solution of the fractional nonlinear Schrödinger equation. Physica Lett. A. 372(5):553-558.

Su WH, Yang XJ, Jafari H, Baleanu D (2013). Fractional complex transform method for wave equations on cantor sets with in local fractional differential operator. Adv. Diff. Equ. 1:1-8.

Sun HH, Abdelwahab AA, Onaral B (1984). Linear approximation of transfer function with a pole of fractional order. IEEE Trans. Automatic Control 29(5):441-444.

Wang Q (2008). Homotopy perturbation method for fractional KdV-Burgers equation. Chaos Solitons Fractals 35(5):843-850.

Wazwaz AA (2008). Study on linear and nonlinear Schrödinger equations by the variational iteration method. Chaos Solitons Fractals 37(4):1136-1142.

Yang AM, Zhang YZ, Long Y (2013a). The Yang-Fourier transforms to Heat-Conduction in a Semi-Infinite fractal BAR. 17(3):707-713.

Yang XJ, Baleanu D (2013). Fractional heat conduction problem solved by Local fractional variation iteration method. Thermal Sci. 17(2):625-628.

Yang XJ, Baleanu D, Khan Y, Mohyud-Din ST (2014). Local fractional variational iteration method for diffusion and wave equations on cantor sets. Romanian J. Phys. 59(1-2):36-48.

Yang XJ, Baleanu D, Zhong WP (2013b). Approximate solutions for Diffusion equations on cantor space-time. Proc. Romanian Acedemy Series A. 14(2):127-133.

Yang XJ, Srivastava HM, He JH, Baleanu D (2013c). Cantor-type Cylindrical-Coordinate fractional derivatives. Phys. A. 377(28):1696-1700.

Zhang YZ, Yang AM, Long Y (2014). Initial boundary value problem for fractal Heat equation in the Semi-infinite Region by Yang-Laplce transform. Thermal Sci. 18(2):677-681.

Zhao CG, Yang AM, Jafari H, Haghbin A (2014). The Yang-Laplace transform for solving He IVPs with local fractional derivative. Abst. Appl. Anal. Article ID 386459, P. 5.

academicJournals

Vol. 10(11), pp. 351-358, 16 June, 2015
DOI: 10.5897/IJPS2015.4356
Article Number: D38B8DE53647
ISSN 1992 - 1950

http://www.academicjournals.org/IJPS

International Journal of Physical Sciences

Full Length Research Paper

Outdoor performance analysis of a monocrystalline photovoltaic module: Irradiance and temperature effect on exergetic efficiency

Cheikh El Banany ELHADJ SIDI[1]*, Mamadou Lamine NDIAYE[1], Ababacar NDIAYE[1,2] and Papa Alioune NDIAYE[1]

[1]Centre International de Formation et de Recherche en Energie Solaire (CIFRES)-Ecole Supérieure Polytechnique-UCAD, BP 5085 Dakar-Fann, Sénégal.
[2]Department de Physique, Université Assane Seck de Ziguinchor BP: 523 – Ziguinchor, Senegal.

Received 24 April, 2015 ; Accepted 26 May, 2015

Studies realized on the performance of photovoltaic modules have shown that analysis of the effect of meteorological parameters is crucial in prediction and evaluation of performances; and production of solar systems. This paper highlights the performing analysis of a monocrystalline silicon photovoltaic module. The aim of this work is to study the effect of irradiance and temperature on module performance in a real environment. The variation of the exergy efficiency as a function of the module temperature on a day is presented. The electrical exergy rate and the thermal exergy losses rate of the module were examined. The findings of this study show that the exergetic efficiency depends on the variation of the irradiance and temperature during the day. Results give an exergetic efficiency of the module varying from 14.87 to 17.93% per day for monocrystalline 30 Wp PV module. The results also show a variation of exergetic efficiency for the same irradiance and decrease in efficiency with increasing module operating temperature. This decrease is 17.5% for an increase of 10 K (irradiance = 900 W/m^2). The thermal exergy losses rate increases with the difference between the module's operating temperature and the ambient temperature. It reaches its maximum (3.36 W) for a temperature difference equal to 28.9 K.

Key words: Exergy, monocrystalline photovoltaic, performance analysis, efficiency, temperature, thermal exergy Losses, Outdoor.

INTRODUCTION

Fossil resources into reserves diminish substantially. Moreover, their use emits into the atmosphere the carbon dioxide gas which is recognized as one of the leaders of global warming. The global energy situation increasingly critical allowed a resurgence of interest in the scientific community for the use of sources of clean and / or renewable energy instead of traditional energy sources. Renewable energy sources contribute more to meeting energy needs. Among renewable technologies, solar systems are best suited to cover certain energy needs.

*Corresponding author. E-mail :benany17@gmail.com, Tel: +221776902924.

Indeed, the climate of Dakar is known for its long sunny days (8.25 kWh / m² / d to the most favorable month and 4.37 kWh / m² / d for the worst month) (Ould et al., 2007). The design and feasibility of photovoltaic systems mainly depend on the available potential and also the performance of the system under the conditions of the installation site. Production and performance of a photovoltaic module are highly bound to sunlight and cell operating temperature. The evaluation of the effect of the variation of meteorological parameters is extremely important in the prediction and estimation of performances taking into account the actual operating conditions of power systems based on photovoltaic modules. The installed system on a site is likely to behave differently if installed on another place. This difference results from the variation of meteorological parameters (Touati et al., 2013; Kamkird et al., 2012). Temperature plays an important role in the solar photovoltaic conversion process. It directly affects the electrical power of the photovoltaic module and consequently the efficiency of the photovoltaic system. Temperature affects the electrical parameters of the PV generator (module). As a result, the module's operating temperature is an important parameter in assessing and predicting the performance of photovoltaic systems (Radziemska and Kulgmann, 2002; Skoplaki et al., 2008). The prediction of output of the modules must take into account the electrical, physical and thermal properties of the cells, the solar radiation, the weather data and the transfer of heat with the environment (Skoplaki et al., 2008).

The effect of the operating temperature on the performances of a photovoltaic module (polycrystalline silicon) has been studied by Malik et al. (2009) under the conditions of Brunei for a period of 2 years. They found that the maximum power, the efficiency and the module fill factor are degraded at high operating temperatures, but a linear relationship cannot be correlated with different variables. This decrease is due to thermal agitation which also increases the loss of free carriers. For building-integrated photovoltaic (BIPV) modules, analyses of electrical and thermal performances have a great importance and should be taken into account in their implementation. Performances of this kind of photovoltaic modules have been studied by Park et al. (2010) in the standard test conditions (STC) and outdoor actual conditions of implementation. The properties of glass supporting photovoltaic cells and its effect on the temperature of the modules were examined. They concluded that the panels produce more electricity in winter than in summer, and the modules with clear glass are more efficient than those with bronzed glass. The results showed that in the STC, the voltage is reduced by 0.49% and the current increases with 0.01% for the increase of one degree Celsius. However, electricity production decreased by 0.48% in regard to the same increase of temperature.

Monitoring of the production and performances of energy systems based on photovoltaic panels in the real conditions of operation of the specific implementation site is of great importance to estimate the reliability and the production of these systems (Ndiaye et al., 2013a; Van Dyk et al., 2002, 2005; Al-Sabounchi et al., 2013). The purpose of monitoring is to assess the performances of photovoltaic modules and their behavior in the short and long-term. In this work we use the thermodynamic analysis (exergy analysis), which is a tool for assessing the performance of conventional and renewable energy systems. This method is adopted to quantify the thermodynamic losses in the process of converting solar energy into electrical energy. The exergetic analysis is used by many academics in evaluating the performances of energy systems such as power plant gas turbines, the drying processes and cooling etc. (Kotas, 1995). Recently this method of analysis was used in the analysis of based renewables energy systems by several researchers (Dincer and Rosen, 2007; Baskut et al., 2010, 2011; Joshi et al., 2009; Vats and Tiwari, 2012; Xydis, 2012; Sahin et al., 2006). Through the theory, a first search that analyzes the thermodynamic aspects of these systems is that of Koroneos et al. (2003). Specifically, Exergy analysis was applied to photovoltaic systems by several researchers. Regarding the conversion of solar energy systems, Akyuz et al. (2012) proposed an approach to determining the maximum value of solar radiations arriving on the surface of a photovoltaic system in order to evaluate the exergetic efficiency. Their approach involves the position of the sun during the day time and angle of incidence. The results show that the maximum exergetic efficiency corresponds to a low wind speed, a minimum ambient temperature and a high global solar radiation.Using the second law of thermodynamics, Sudhakar and Srivastava (2013) evaluated the energetic and exergetic efficiencies of a photovoltaic solar module (36Wp). The module electrical parameters and those of operation are included in the calculation of energetic efficiency (6-9%) and exegetic efficiency (8-10%). Pandey et al. (2013) examined the performances of polycrystalline silicon modules with exergy analysis. Also, Sarhaddi et al. (2009) have developed an optimization method using exergy analysis to determine the design parameters and optimum performances of a photovoltaic panel. For a wind / PV hybrid system a study was conducted by Xydis (2013) to evaluate the exergetic efficiency. They introduced the exergy capacity factor (EXCF) which is the ratio of net energy provided by the system (kWh) on the total installed capacity (kW) multiplied by the number of hours of the year (h). They identified temperature and strong sunlight losses as the parameters that most affect the performances of photovoltaic modules in the hybrid system.

An obstacle that limits the development of renewable electrical systems is their low efficiency and lack of performance data in terms of the actual environment in locations where they are installed. Production and performances of a photovoltaic module are highly dependent on sunlight and operating temperature of cell (Yang et al., 2007).

Our analysis is performed on a photovoltaic module (30 Wp) whose performance is studied with respect to the variation of meteorological parameters (irradiance and temperature). The short-circuit current, open circuit voltage and module temperature were measured. The results of the analysis of the exergetic efficiency, the electrical exergy rate and the thermal exergy losses rate as function of the increase of the module temperature are presented.

MATERIALS AND METHODS

The methodological approach in this work consist of 3 steps:

(i) Acquisition of meteorological parameters and experimental data for the production of a photovolataic module.
(ii) Analyzing the effect of the irradiance and temperature on photovoltaic module efficiency through exergetic analysis.
(iii) Evaluating the thermal exergy losses rate of the module as function of temperature in sunny and cloudless day.

Exergy analysis is a tool for design and evaluation of energy systems. It is designed to evaluate the systems that begin in equilibrium but do not stay in mutual equilibrium with the environment during the process of energy conversion. Exergy is defined as the measure of the maximum useful work that can be provided by a system interacting with its environment has a pressure P_0 and temperature T_0 (Dincer and Rosen, 2007). Exergy can be associated with several forms of transfers such as the transfer of work, heat, material flow and others (Kotas, 1995). In the case of a system in equilibrium with its environment where conditions of mechanical equilibrium, thermal, electrical etc. are equal to those of the environment, exergy is zero. Exergy has the characteristic that it is destroyed when an irreversible process happens. When an exergetic analysis is performed on a process or system, the thermodynamic imperfections are quantified as quality losses of energy. This analysis method is adopted to identify the thermodynamic losses of energy systems. An important concept in exergy analysis is the exergetic efficiency for assessing the performance of an energy system taking into account the limitations imposed by the second law of thermodynamics.

The output power and the performances of photovoltaic modules are highly depending on sunlight, operating temperature and other weather parameters such as the accumulation of dust, a natural phenomenon characteristic of desert climates. Ndiaye et al. (2013b) have shown the importance of removing dust from the surface of the modules to ensure better performances and efficiency of photovoltaic modules. In our case, the effect of dust is not investigated. Indeed, the module was clean in the period of study. Generally, photovoltaic modules operate in operating conditions different from the operating standard conditions (STC), where the modules operating temperature is often greater than that in the STC. The increase of the ambient temperature and sunlight lead to a growth of the module's operating temperature (T_C) which can be estimated by linear approximation by Kenny formula (Kenny et al., 2006):

$$T_C = T_a + \left(\frac{T_{NOCT} - 20}{G_{NOCT}} \right) G \quad (1)$$

Where G is the irradiance (W/m^2), T_a is the ambient temperature, T_{NOCT} is module temperature under nominal operating conditions (wind speed $= 1\, m/s$, $G_{NOCT} = 800\, W/m^2$ and $T_a = 20\,°C$) and G_{NOCT} is the irradiance under nominal operating conditions.

The generated power and the performances of photovoltaic modules depend on weather parameters such as ambient temperature (T_a), irradiance (G), wind speed (v_w) etc. It also depends on the intrinsic parameters of photovoltaic modules Technology: the short circuit current (I_{sc}), the maximum output current ($I_{\max}$), the open circuit voltage (V_{oc}), the maximum output voltage ($V_{\max}$) and the module surface (A). The output exergy rate of the photovoltaic module (Ex_{PV}) is the electrical exergy rate (Ex_{ele}) which is equal to the electric power generated by the module:

$$Ex_{PV} = Ex_{ele} \quad (2)$$

The electrical exergy rate is the maximum power generated by the photovoltaic module. It is given by Equation (3) (Ndiaye et al., 2014; Notton et al., 2005).

$$Ex_{ele} = FF \times V_{oc} \times I_{sc} \quad (3)$$

The solar radiation exergy rate ($Ex_{radiation}$) which reaches the module surface (A) is expressed according to the theorem of Patela (Patela, 2003) and given by the following expression (temperature is expressed in Kelvin subsequently):

$$Ex_{radiation} = AG \left(1 - \frac{4}{3}\left(\frac{T_a}{T_s} \right) + \frac{1}{3}\left(\frac{T_a}{T_s} \right)^4 \right) \quad (4)$$

Where T_s is the sun's temperature which is equal to $5762\ K$.

The thermal exergy losses rate through the solar conversion process is in the form of heat loss from the surface of the module to the outside. Photovoltaic modules heat up because of their exposure to sunlight and emit quantity of heat into the environment. This heat source is not in equilibrium with the environment; and consequently possesses an exergy which represents the thermal losses of the photovoltaic module (Akyuz et al., 2012).

$$Ex_{losses} = Q \left(1 - \frac{T_a}{T_C} \right) \quad (5)$$

The convective heat transfer rate is given by the following equation:

$$Q = h_{ec} A (T_C - T_a) \quad (6)$$

Table 1. specifications (STC) of photovoltaic module used in experimentation.

Specifications	Values
Nominal Peak power (Watts)	30
Short-circuit current (Ampers)	2.24
Open-circuit voltage (Volts)	22.50
Fill Factor (-)	0.72
PV cell surface (cm²)	49
Cells number (-)	36

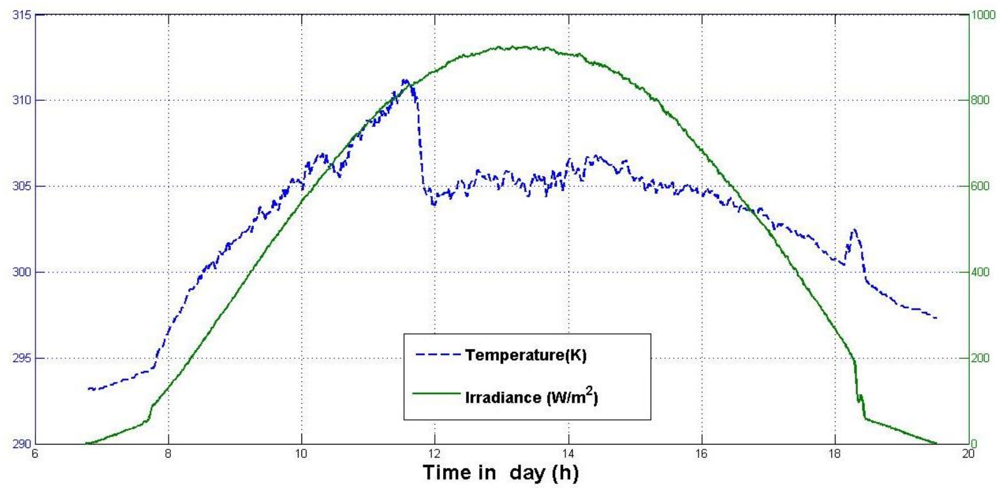

Figure 1. Daily variation of irradiance and ambient temperature (one sunny day).

The parameter (h_{ec}) is the convective heat transfer coefficient between environment and module and whose expression is given by:

$$h_{ec} = 5.7 + 3.8 v_w \tag{7}$$

In this work the wind speed was not measured. It is taken under nominal operating conditions ($v_w = 1\ m/s$) to quantify the heat loss of the module.

RESULTS AND DISCUSSION

In order to evaluate the performances of the photovoltaic module, we use the exergetic efficiency. The exergetic efficiency of solar energy conversion process into electrical energy (Equation 8) is defined as the ratio of exergy useful (electrical exergy rate) Equation (3) on exergy of the solar radiation rate Equation (4):

$$\varepsilon_{PV} = \frac{\mathrm{FF} \times V_{oc} \times I_{sc}}{AG\left(1 - \frac{4}{3}\left(\frac{T_a}{T_s}\right) + \frac{1}{3}\left(\frac{T_a}{T_s}\right)^4\right)} \tag{8}$$

The data of irradiance and ambient temperature are measured at the Higher Polytechnic School (ESP) of the Dakar University in Senegal (17.28° West longitude and 14.43° North latitude). In the same environment, a single crystal photovoltaic module (30 Wp) was installed and the short-circuit current, the open circuit voltage of the module and its temperature was collected. The characteristics of a photovoltaic module used in the experiment are given in Table 1.

Irradiance and module temperature are plotted for a day in Figure 1. Temperature increases and decreases simultaneously with irradiation. Consequently in a real environment it is difficult to discern the effect of temperature on performances of the photovoltaic module. The evolution of exergy of the solar radiation rate and electrical exergy rate are plotted for one sunny day in the Figure 2. The electrical exergy rate increases from zero to 7 h 15 min until 26.7 W at 13 h 22 min and then decreases again to zero at 19 h 32 min.

The variation for this day of the exergetic efficiency is given in Figure 3. It depends on the time of day and depends on the sunshine and temperature simultaneously. In fact it varies from 14.87 to 17.93% of irradiance and temperature combination of the day.

In order to analyze the effect of temperature on

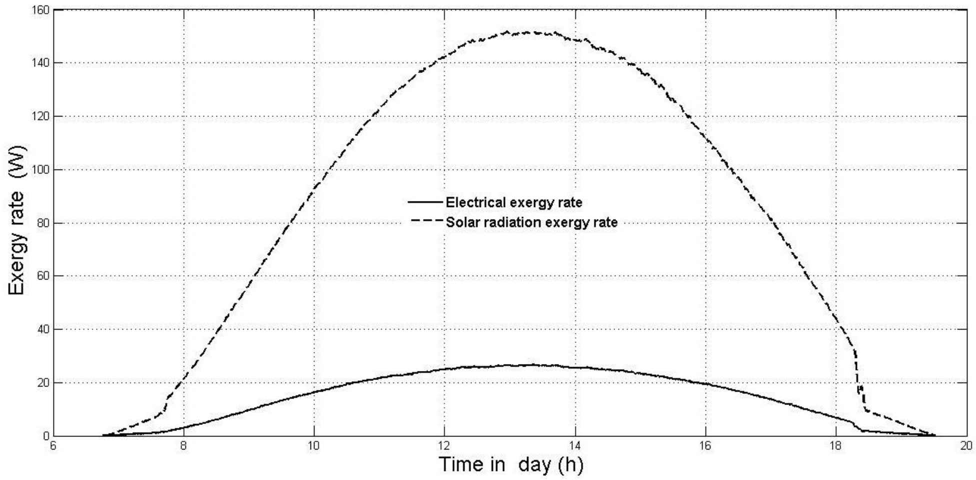

Figure 2. Daily variation of electrical exergy rate and solar radiation exergy rate (one sunny day).

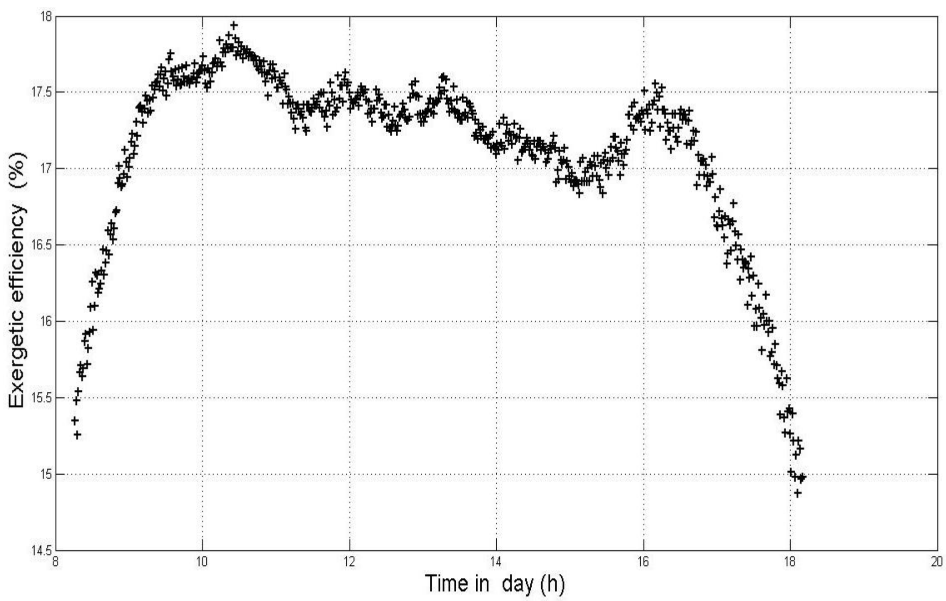

Figure 3. Daily variation of exergetic efficiency (one sunny day).

exergetic efficiency, data from 6 to 18 June 2012 are used and the data corresponding to the irradiances 500 and 900 W/m^2 are selected. In Figure 4, the variation of exergetic efficiency as a function of temperature for the irradiances of 500 and 900 W/m^2 respectively is shown. From Figures 3 and 4, we can see that the exergetic efficiency of the module is not constant and varies in a real environment according to the instantaneous irradiance and temperature. For an irradiance of 500 W/m^2, the efficiency decreases by 4.2% to an increase of 9.3 K (316.2 to 325.5 K) module temperature; while for 900 W/m^2, the efficiency decreases by 17.5% to an increase of 10 K (329.9 to 339.9 K). This results show that for a constant irradiance, the exergetic efficiency decreases with increasing temperature. The dependence of the efficiency on rising in temperature is greater when the irradiance is larger. As part of a large photovoltaic installation of several kWp to MWp, this reduction in the yield due to the operating temperature can greatly affect the total output of the system.

The thermal exergy losses rate during the conversion process is quantified using the Equation (5). Its variation during the day is given in Figure 5. It can be seen that the maximum of the heat losses magnitude corresponds to the hours of the day when the irradiance and module

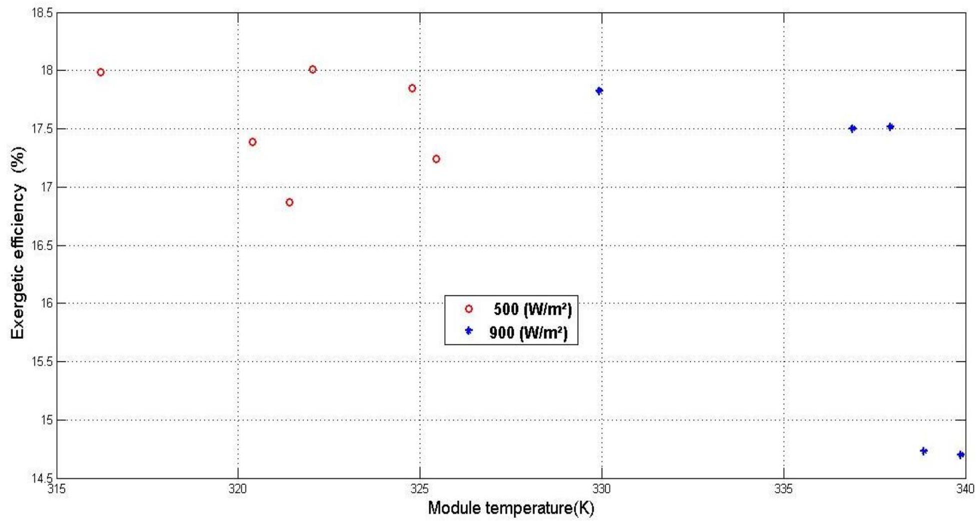

Figure 4. Exergetic efficiency versus module temperature for irradiance values equal to 500 and 900 (W/m^2).

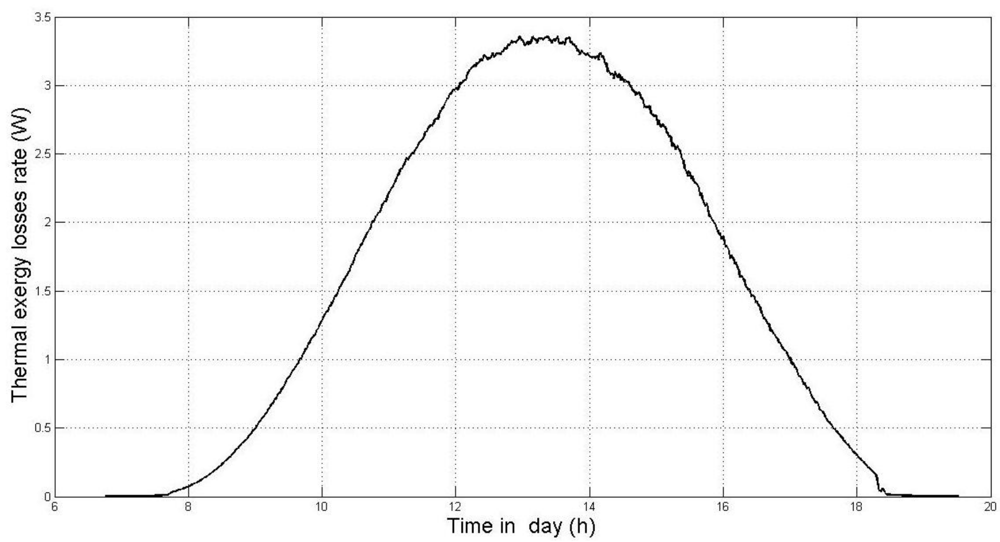

Figure 5. Daily variation of the thermal exergy losses rate (one sunny day).

temperature are maximal. The variation of the thermal exergy losses rate depending on the difference between the module temperature and the ambient temperature ($T_C - T_a$) is given in Figure 6. From this figure it is clear that the thermal exergy losses rate increases with the difference between T_C and T_a. When this difference reaches its maximum in the daytime (28.9 K), the thermal exergy losses rate its maximum which is equal to 3.36 W.

In order to better harness the waste heat from the module, other researchers like Dubey et al. (2009) proposed the use of hybrid photovoltaic and thermal module (PV\T). This device converts the absorbed solar radiation into electricity and heat can be used simultaneously to heat water or air. PV\T system consists of a photovoltaic module integrated with a solar heat collector providing heat. The PV\T system benefits from the heat to generate more energy per unit area. Integrating PV\T systems can be a viable way that produces electricity in combination with air or hot water for installations in buildings. Abdolzadeh and Ameri (2009) proposed to consider installing water spray systems on photovoltaic panels in pumping systems to

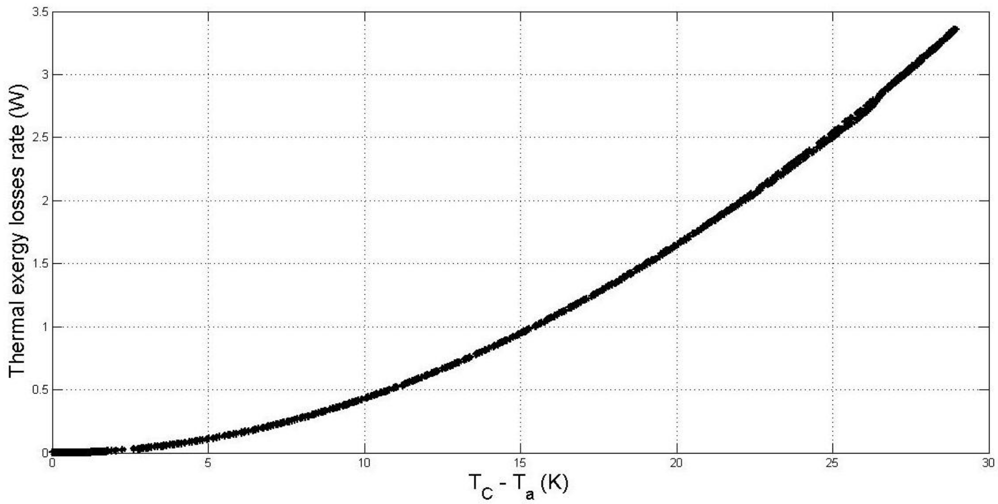

Figure 6. Variation of the thermal exergy losses rate versus (one sunny day).

improve their performances by reducing the temperature of the cells through the glass and clean the dust. Their results showed that irrigation may reduce the operating temperature of 23°C and increase the yield of 3.26%.

Conclusion

Exergy analysis was performed to a monocrystalline photovoltaic module (30 Wp) in a real environment. The effect of irradiance and temperature on performances was examined and produced electrical exergy rate and thermal exergy losses rate of the photovoltaic module were quantified for one day. The results of this study confirmed the dependency of the exergetic efficiency of the module to the variation of the irradiance and temperature. These findings can be summarized as followed:

(i) The exergetic efficiency of the module varies from 14.87 to 17.93% as claimed in irradiance and temperature combination of the day.
(ii) For the same irradiance, the exergetic efficiency decreases with the increase in module temperature. This decrease is 17.5% for an increase of 10 K (329.9 to 339.9 K) for constant irradiance about 900 W/m^2.
(iii) The thermal exergy losses rate increases with the difference between the module temperature and the ambient temperature. It reaches its maximum of 3.36 W for a temperature difference equal to 28.9 K.

However, the exergetic efficiency is a function of the combination irradiance- temperature in a day. Furthermore, these parameters are randomized and depended on a season and a time of day. Therefore, it is difficult to discern the effect of each parameter separately on PV module performance in a real environment.

Conflict of Interest

The authors have not declared any conflict of interest.

REFERENCES

Abdolzadeh M, Ameri M (2009). Improving the effectiveness of a photovoltaic water pumping system by spraying water over the front of photovoltaic cells. Renewable Energy 34(1):91–96. http://dx.doi.org/10.1016/j.renene.2008.03.024

Akyuz E, Coskun C, Oktay Z, Dincer I (2012). A novel approach for estimation of photovoltaic exergy efficiency. Energy. 44(1):1059–1066. http://dx.doi.org/10.1016/j.energy.2012.04.036

Al-Sabounchi AM, Yalyali SA, Al-ThaniHamda A (2013). Design and performance evaluation of a photovoltaic grid-connected system in hot weather conditions. Renewable Energy. 53:71–78. http://dx.doi.org/10.1016/j.renene.2012.10.039

Baskut O, Onder O, Leyla O (2010). Effects of meteorological variables on exergetic efficiency of wind turbine power plants. Renewable Sustainable Energy Rev. 14(9):3237–3241. http://dx.doi.org/10.1016/j.rser.2010.06.002

Baskut O, Onder O, Leyla O (2011). Second law analysis of wind turbine power plants: Cesme, Izmir example. Energy 36(5):2535–2542. http://dx.doi.org/10.1016/j.energy.2011.01.047

Dincer I, Rosen M (2007). Exergy: Energy, Environment and Sustainable Development. Elsevier Science, ISBN: 978-0-08-044529-8:472.

Dubey Swapnil, Sandhu GS, Tiwari GN (2009). Analytical expression for electrical efficiency of PV/T hybrid air collector. Appl. Energy 86(5):697–705. http://dx.doi.org/10.1016/j.apenergy.2008.09.003

Joshi AS, Dincer I, Reddy BV (2009). Thermodynamic assessment of photovoltaic systems. Solar Energy 83(8):1139–1149. http://dx.doi.org/10.1016/j.solener.2009.01.011

Kamkird P, Ketjoy N, Rakwichian W, Sukchai S (2012). Investigation on temperature coefficients of three types photovoltaic module technologies under thailand operating condition. Procedia Eng. 32:376–383. http://dx.doi.org/10.1016/j.proeng.2012.01.1282

Kenny RP, Dunlop ED, Ossenbrink HA, Müllejans H (2006). A practical method for the energy rating of c-Si photovoltaic modules based on standard tests. Progress in Photovoltaics: Res. Appl. 14(2):155–166. DOI: 10.1002/pip.658

Kotas TJ (1995).The exergy method of thermal plant analysis. Kerieger publishing company.

Koroneos C, Spachos T, Moussiopoulos N (2003). Exergy analysis of renewable energy sources. Renewable Energy. 28(2):295–310. http://dx.doi.org/10.1016/S0960-1481(01)00125-2

Malik AQ, Ming Lim C, Sheng Tan K, Blundell M (2009). Influence of temperature on the performance of photovoltaic polycrystalline silicon module in the Bruneian climate. ASEAN. J. Sci. Technol. Dev. 26(2):63–74.

Ndiaye A, Kébé CMF, Ndiaye PA, Charki Abdérafi KA, Sambou V (2013a). A Novel Method for Investigating Photovoltaic Module Degradation. Energy Procedia 36:1222–1231.

Ndiaye A, Kébé CMF, Ndiaye PA, Charki A, Kobi A, Sambou V (2013b). Impact of dust on the photovoltaic (PV) modules characteristics after an exposition year in Sahelian environment: The case of Senegal. Int. J. Phys. Sci. 8(21):1166-1173.

Ndiaye A, Kébé CMF, Ndiaye PA, Charki A, Sambou V, Kobi A, (2014). Degradation evaluation of crystalline-silicon photovoltaic modules after a few operation years in a tropical environment. Solar Energy 103:70–77. http://dx.doi.org/10.1016/j.solener.2014.02.006

Notton G, Cristofari C, Mattei M, Poggi P (2005). Modelling of a double-glass photovoltaic module using finite differences. Appl. Thermal Eng. 25(17–18):2854–2877. http://dx.doi.org/10.1016/j.applthermaleng.2005.02.008

Ould Bilal B, Sambou V, Kébé CMF, Ndongo M, Ndiaye PA (2007). Etude et modélisation du potentiel solaire du site de Nouakchott et de Dakar. J. Sci. 7(4):57–66.

Pandey AK, Tyagi VV, Tyagi SK (2013). Exergetic analysis and parametric study of multi-crystalline solar photovoltaic system at a typical climatic zone. Clean Technol. Environ. Policy. 15(2):333-343.

Park KE, Kang GH, Kim HI, Yu GJ, Kim JT (2010). Analysis of thermal and electrical performance of semi-transparent photovoltaic (PV) module. Energy 35(6):2681–2687. http://dx.doi.org/10.1016/j.energy.2009.07.019

Patela R (2003). Exergy of undiluted thermal radiation. Solar Energy 74(6):469–488. http://dx.doi.org/10.1016/S0038-092X(03)00226-3

Radziemska E, kulgmann E (2002). Thermally affected parameters of the current-voltage characteristics of silicon photocell. Energy conver. manage. 43:1889–900. http://dx.doi.org/10.1016/S0196-8904(01)00132-7

Sahin AD, Dincer I, Rosen MA (2006). Thermodynamic analysis of wind energy. Int. J. Energy Res. 30(8):553–566. DOI: 10.1002/er.1163

Sarhaddi F, Farahat S, Ajam H, Behzadmehr A (2009). Exergetic Optimization of a Solar Photovoltaic Array. J. Thermodyn. 11 pages. http://dx.doi.org/10.1155/2009/313561

Skoplaki E, Boudouvis AG, Palyvos JA (2008). A simple correlation for the operating temperature of photovoltaic modules of arbitrary mounting. Solar Energy Mater. Solar Cells. 92(11):1393–1402. http://dx.doi.org/10.1016/j.solmat.2008.05.016

Sudhakar K, Srivastava T (2013). Energy and exergy analysis of 36W solar photovoltaic module. Int. J. Ambient Energy. DOI: 10.1080 /01430750.2013.770799

Touati FA, Al-Hitmi MA, Bouchech HJ (2013). Study of the Effects of Dust, Relative Humidity, and Temperature on Solar PV Performance in Doha: Comparison Between Monocrystalline and Amorphous PVS. Int. J. Green Energy. 10(7):680-689.DOI:10.1080/15435075.2012.692134

Van Dyk EE, Meyer EL, Vorster FJ, Leitch AWR (2002). Long-term monitoring of photovoltaic devices. Renewable Energy. 25(2):183–197. http://dx.doi.org/10.1016/S0960-1481(01)00064-7

Van Dyk EE, Gxasheka AR, Meyer EL (2005). Monitoring current–voltage characteristics and energy output of silicon photovoltaic modules. Renewable Energy. 30(3):399–411. http://dx.doi.org/10.1016/j.renene.2004.04.016

Vats K, Tiwari GN (2012). Energy and exergy analysis of a building integrated semitransparent photovoltaic thermal (BISPVT) system. Appl. Energy 96:409–416. http://dx.doi.org/10.1016/j.apenergy.2012.02.079

Xydis G (2012). The wind chill temperature effect on a large-scale PV plant-an exergy approach. Progress Photovoltaics Progress Res. 21(8):1611–1624. DOI: 10.1002/pip.2247

Xydis G (2013). On the exergetic capacity factor of a wind-solar power generation system. J. Cleaner Prod. 47:437–445. http://dx.doi.org/10.1016/j.jclepro.2012.07.014

Yang HX, Lu L, Zhou W (2007). A novel optimization sizing model for hybrid solar-wind power generation system. Solar Energy. 81(1):76–84. http://dx.doi.org/10.1016/j.solener.2006.06.010

academicJournals

Vol. 10(11), pp. 359-363, 16 June, 2015
DOI: 10.5897/IJPS2015.4358
Article Number: A96694253649
ISSN 1992 - 1950

http://www.academicjournals.org/IJPS

International Journal of Physical Sciences

Full Length Research Paper

Microwave propagation attenuation due to earth's atmosphere at very high frequency (VHF) and ultra-high frequency (UHF) bands in Nsukka under a clear –air condition

Ernest Benjamin Ikechukwu Ugwu[1,2]*, Maureen Chioma Umeh[1] and Obiageli Josephine Ugonabo[1]

[1]Department of Physics and Astronomy, University of Nigeria, Nsukka, Enugu State, Nigeria.
[2]Natural Science Unit, University of Nigeria, Nsukka, Enugu State, Nigeria.

Received 26 April, 2015; Accepted 1June, 2015

The microwave propagation attenuation due to earth's atmosphere under a clear-air condition for fade depth of 10 dB was investigated using refractivity data calculated from weather vagaries measurement carried out between January and December 2008. The International Telecommunication Union-Radiocommunication Sector (ITU-R) model for multipath fading for small percentage of time with link distance of 100 km was used. The result showed that at this distance, the refractivity gradient has a strong correlation of 0.747 with percentage of time that the fade depth was exceeded. It was also observed that the percentage of time that the fade depth was exceeded increases with frequency until about 1.2GHz when the result becomes unreliable.

Key words: Attenuation, fade depth, microwave, multipath fading, refractivity gradient.

INTRODUCTION

The meteorological effect on microwave signals especially at very high frequency (VHF) and ultra-high frequency (UHF) band is very significant. Several clear-air effects (Oyedum, 2007), such as, sub-refraction, super-refraction, ducting and scattering due to variations in tropospheric condition can seriously enhance or degrade the quality of reception of a microwave communication link (Ayantunji and Okeke, 2011; Falodun and Okeke, 2013).

There are several sources of signal attenuations that can affect a microwave signal in the troposphere. These attenuations include beam spreading (defocusing), antenna decoupling, atmospheric gaseous absorption, rain attenuation, tropospheric scattering under a clear-air-condition, and multipath fading among others. Most of these mechanisms can occur by themselves or in combination with each other (ITU-R P.530-8).

Multipath fading is the most common type of fading encountered, particularly on line-of-sight (LOS) radio links. It is the principal cause of dispersion, which is particularly troublesome on digital troposcatter and high-bit-rate LOS links. For an explanation of atmospheric

*Corresponding author. E-mail: ernestb.ugwu@unn.edu.ng, Tel: +2348066953787.

multipath fading, we must turn to the refractive index gradient. As the gradient varies, multipath fading results, owing to the:

1. Interference between direct rays and the specula component of a ground-reflected wave;
2. The non-specula component of the ground-reflected wave;
3. Partial reflections from atmospheric sheets or elevated layers;
4. Additional direct wave paths and non-reflected paths.

One or more of these multipath fading mechanisms may occur at a time. Of interest to the radio link design engineer is the fading rate (the number of fades per unit time) and the fading depth (the magnitude of the variation of the signal intensity at the receiver from its free-space value expressed in decibels).

Fade depths can exceed 20 dB, particularly on longer LOS paths and more than 30 dB on longer troposcatter paths (Freeman, 2007; Grabner et al., 2011). Fade durations of up to several minutes or more can be expected. Often multipath fading is frequency selective and the best technique for mitigation is frequency diversity. For effective operation of frequency diversity, sufficient frequency separation is required between the two transmit frequencies to provide sufficient de-correlation.

Rain intensity, refractivity gradient and annual mean temperature are critical parameters affecting link performance (Agba et al., 2011). Fades due to atmospheric multipath are very important, particularly for point-to-point microwave links. The effect occurs predominantly in higher-humid areas during night time hours, with coastal areas being particularly susceptible (Seybold, 2007). Like refraction, atmospheric multipath only affects paths that are very nearly horizontal. Atmospheric multipath is primarily observed over very flat terrain; irregular terrain makes formation of a uniform atmospheric layer unlikely. The impact of this kind of multipath on terrestrial point-to-point microwave links was studied by Bell Laboratories in the 1960s and 1970s. Models (Morita model, 1970 used in Japan, Barnett-Vigants models, 1970 and 1972 widely used in the United States and Segal model, 1992 used in Canada, ITU-R models used worldwide) were developed for predicting the multipath distribution effects on terrestrial LOS links (Agba et al., 2011). The ITU-R model is periodically updated. An evaluation of the prediction equation for the revised and previous ITU-R models and other regional models like Barnett-Vigants and Morita models showed that the revised ITU model (2001) slightly performed better than the other models for both overland and coastal/overwater links (Olsen et al., 2003). The revised ITU model (2001) is adopted in this work.

The ITU model for atmospheric multipath has two different formulations for low probability of fade and another formulation for all fade probabilities. For most applications, the low fade probability is apt. In addition to providing multipath fade depth predictions, the ITU model also provides a model for multipath signal enhancement. The enhancement model is not presented herein, but it may be of interest in assessing the potential for interference in frequency re-use application.

The available data for multipath fading is usually based on data from coastal areas because the effect occurs predominantly in higher humid region. This might not be entirely true since tropospheric refractive index has a distinct dependence on weather vagaries (air temperature, air pressure and relative humidity) in Nsukka, Nigeria (Ayantunji and Umeh, 2010). Spatial distribution of the refractive index of the air, especially its vertical profiles, affects the propagation of electromagnetic waves in atmosphere (Grabner et al., 2013). In the hinterland areas with large concentration, it is important that the effect of multipath on radio frequency propagation be carried out to enhance the communication system.

METHODOLOGY AND INSTRUMENTATION

The Centre for Basic Space Science (CBSS), University of Nigeria, Nsukka, Nigeria provided the data for determining the radio refractivity gradient. The CBSS has Vantage Pro2 automatic weather stations installed on Nigeria Telecommunication (NITEL) mast at the ground level (0m height) and at 100 m height that collect data every 30 s via the integrated sensor suite (ISS) and the data are transmitted to the console at 860 MHz. A GPS was used to determine the altitude of the site. Other data used were hypothetical and this was achieved by keeping some variables (like frequency, heights of the antennas, path separation, and fade depth) in the ITU model (2001) constant while one is varied.

For a clear-air condition (that is, atmosphere without rain, snow, fog or other conditions) radio refractivity expressed by equation (1) was computed for various months having calculated e_s and e using Equations (3) and (2) respectively.

The gradient of refractivity (dN) was calculated from the computation done for all values on the surface (0m) and at a height of 100 m above the surface level.

Tropospheric radio refractivity, N, and partial vapour pressure, e, are defined by the ITU-R (2003) formula in equations 1 and 2 respectively:

$$N = \frac{77.6P}{T} + 3.73 \times 10^5 \frac{e}{T^2} \quad (1)$$

$$e = R_h e_s / 100 \quad (2)$$

Where P is atmospheric pressure (hPa), T is temperature (K), R_h is relative humidity (%) and e_s is saturated vapour pressure (hPa) at a given temperature, t (°C) and is obtained from:

$$e_s = 6.112 exp\, 17.5t/(t + 240.97) \quad (3)$$

For a clear-air condition (that is, atmosphere without rain, snow, fog or other conditions) radio refractivity expressed by Equation (1) was computed for various months after calculating e_s and *e*. The gradient of refractivity (dN) was calculated from the computation

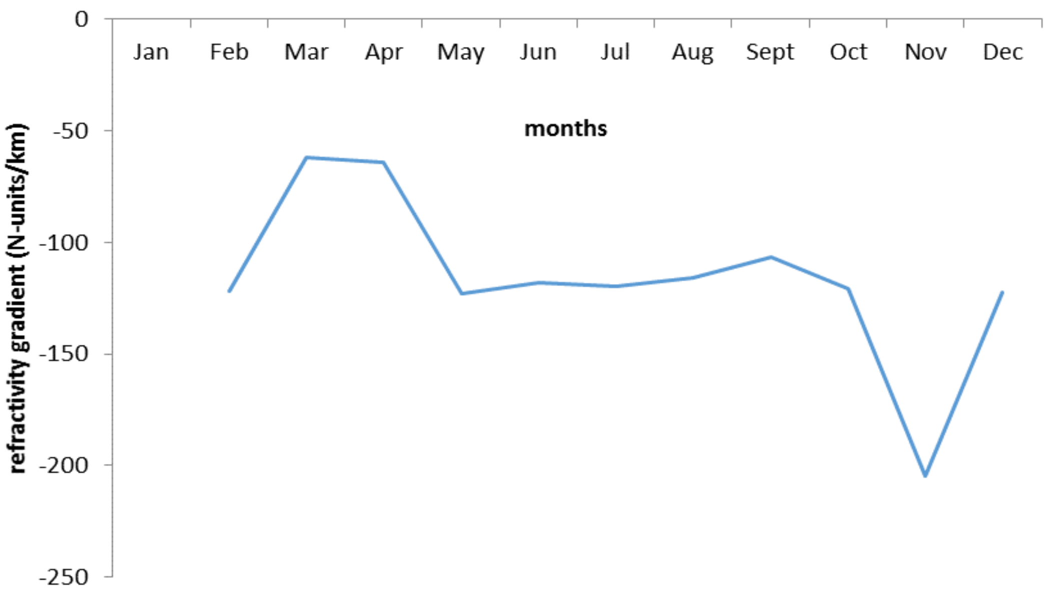

Figure 1. Seasonal variation of refractivity gradient.

done for all values on the surface (0 m) and at a height of 100 m above the surface level.

The first step in applying the ITU-R, 2001 for small percentages is to determine geoclimatic factor, K given by:

$$K = 10^{-3.9-0.003dN_1} s_a^{-0.42} \quad (4)$$

where dN_1 is the point refractivity gradient in the lowest 65m of the atmosphere not exceeded for 1% of an average year, and s_a is the area terrain roughness defined as the standard deviation of terrain heights (m) within a 110 km × 110 km area with a 30 s resolution (e.g. the Globe "gtopo30" data). The area was aligned with the longitude such that the two equal halves of the area are on each side of the longitude that goes through the path centre. The geoclimatic factor, K was determined using equation 5 since s_a is not available for Nsukka.

$$K = 10^{-4.2-0.0029dN_1} \quad (5)$$

The second step is to determine the magnitude of the path inclination, $|\varepsilon_p|$ given by:

$$|\varepsilon_p| = (|h_r - h_e|)/d \quad (6)$$

where $|\varepsilon_p|$ is the path inclination (mrad), h_r and h_e are the heights (in metres above sea-level or some other reference height) of the receiving and transmitting antenna respectively and d is the link distance, taht is, the separation between the two antennas (km).

For detailed link design, the percentage time or "worst month" outage probability, P_w for which a particular fade depth A (dB) is exceeded is given by:

$$P_w = Kd^{3.2}(1+|\varepsilon_p|)^{-0.97} \times 10^{0.032f-0.00085h_L-A/10} \% \quad (7)$$

where d is the path length (km), f is the frequency (GHz), h_L is the altitude of the lower antenna (m), and A is the fade depth (dB). P_w is expressed in % or seconds.

For quick design however, we used Equation (8):

$$P_w = Kd^{3.0}(1+|\varepsilon_p|)^{-1.2} \times 10^{0.033f-0.001h_L-A/10} \% \quad (8)$$

The path inclination, $|\varepsilon_p|$ and percentage time, P_w of attenuation for detailed design for which a particular fade depth is said to be exceeded were also computed. To calculate these, the following values were assumed; h_r = 20m; h_e = 150 m; d = 100 km (100,000 m); f = 1 GHz (1000 MHz); h_L = 20 m; A = 10 dB/m. Due to the large values, excel was used for these calculations.

RESULTS AND DISCUSSION

Figure 1 shows seasonal variation of refractivity gradient which maintains almost a constant value in the rainy season. This pattern of variation is probably due to the high humidity during the rainy season. The refractivity gradient peaked in the month of March which is an indication of the peak of dry season at Nsukka and decreases gradually in subsequent months of the year. Grabner et al. (2012) observed the largest values of refractivity index structure constant in the summer months and the least values in the winter months in Czech Republic. This indicates that the radio refractivity values vary with climatic zones as well as with the seasons of the year (Falodun and Okeke, 2013).

Figure 2 shows variation of percentage of time of attenuation with refractive gradient at 10 dB fade depth averaged over each month. From this we can deduce that the more negative the refractivity gradient the more

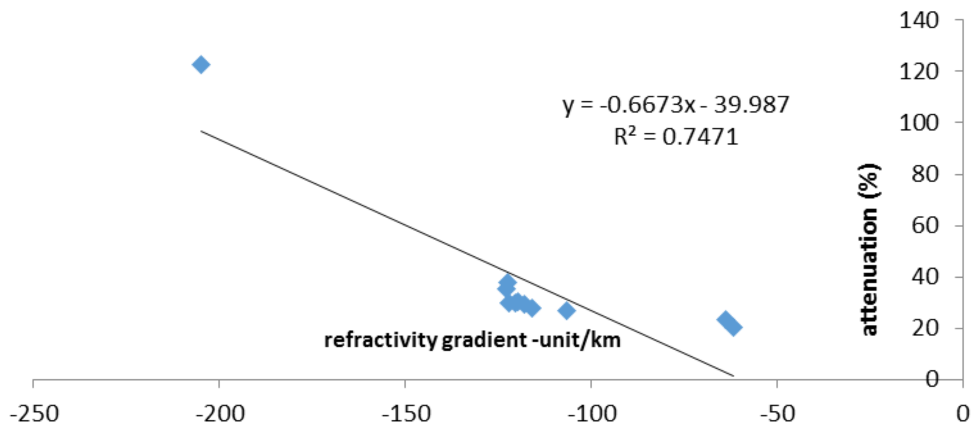

Figure 2. Variation of percentage of time for attenuation with refractivity gradient at 10 dB fade depth.

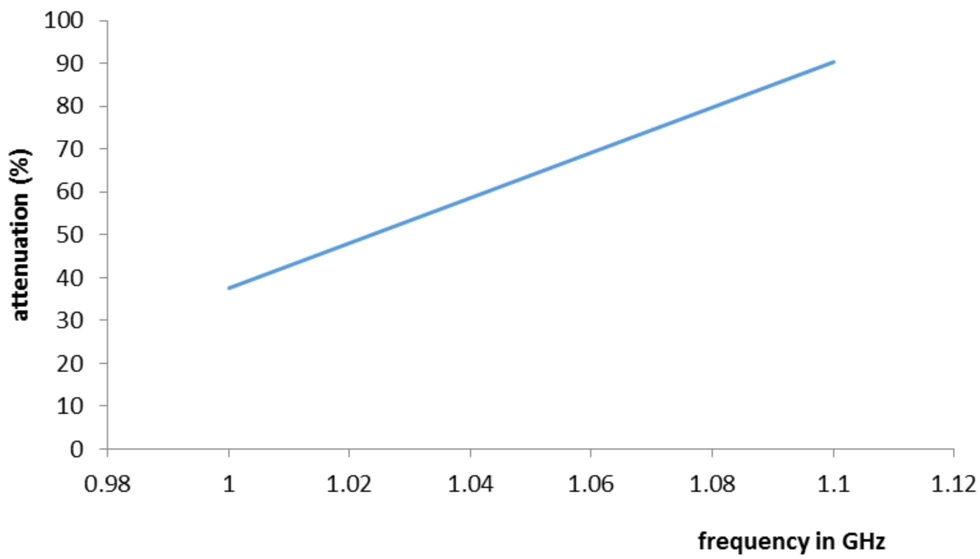

Figure 3. Variation of attenuation with frequency.

the attenuation. This implies lesser refractivity gradient and greater attenuation. The relationship:

$$P = -0.667dN - 39.98 \qquad (9)$$

gives the relationship between percentage of time and refractivity gradient as obtained from the graph. A regression coefficient R^2 = 0.747 was obtained between the two variables. This shows high correlation.

Figure 3 shows variation of attenuation with frequency which was obtained from simulated data given in Table 1. This was obtained by varying the frequency using Equation (8) while other parameters remained constant. This shows that as frequency of transmission increases the attenuation increases. At frequencies greater than 1.2 GHz attenuation tends to infinity, which suggests that the study under clear-air condition is of little or no importance above this frequency. Under a clear-air condition, attenuation is proportional to frequency at VHF and UHF

Table 1. Variation of attenuation with frequency.

Frequency (GHz)	Attenuation due to clear-air condition (%)
1.0	37.59
1.02	48.18
1.04	58.76
1.06	69.34
1.08	79.90
1.10	90.51

bands and in line sections and low-loss adapters add significant contributions to the uncertainty of power measurements when the calorimeter correction factor is determined (Xiaohai and Crowley, 2011). An attempt was made to study the effects of variation of antennas' heights and the link distance at fade depth and frequency. No reasonable effect was observed.

We shall subsequently attempt to study in detail the effects of variation of the antenna height and the link distance at the fade depth and the frequency.

Conclusion

The results obtained from the study of microwave propagation attenuation due to earth's atmosphere under a clear-air condition for a fade depth of 10 dB suggest that refractivity gradient and percentage of time of attenuation at Nsukka have a very strong correlation of 0.747. This agrees with the results obtained by Westwater et al. (1990) in which there were a strong agreement between measurements and calculations with the least correlation at 0.9. They also observed that attenuation distributions are dependent on location and season

Also, the percentage of time of attenuation increases with increase in frequency unto about 1.2 GHz when the result becomes unreliable. Grabner et al. (2013) tried to model multipath propagation conditions but had unsatisfactory results. Horizontal spatial distribution of refractivity can be complex (Barrios, 1992), hence vertical refractivity profiles are not enough to describe propagation path under multipath conditions. The results obtained may improve radio communication system in Nigeria since only 25.82% of the entire land mass of Niger state, for example, has television signal coverage (Ajewole et al., 2013).

Conflict of Interest

The authors have not declared any conflict of interest.

REFERENCES

Agba BL, Ben-Sik-Ali O, Morin R, Bergeron G (2011). Recent evolution of ITU method for prediction of multipath fading on terrestrial microwave links. Progress in Electromagnetics Res. Symposium Proc. Marrakesh, Morocco, Mar. 20-23:1375.

Ajewole MO, Oyedum OD, Adediji AT, Moses AS, Eiche JO (2013). Spatial variability of VHF/UHF electric field strength in Niger State, Nigeria. Int. J. Digital Info. Wireless Comm. (IJDIWC) 3(3):231-239. The Society of Digital Information and Wireless Communications, 2013 (ISSN: 2225-658X).

Ayantunji BG, Okeke PN (2011) Diurnal and seasonal variation of surface refractivity over Nigeria. Progress in Electromagnetic Res. B. 30:201-222.

Ayantunji BG, Umeh MC (2010). Statistical study of the dependence of tropospheric refractive index on different weather vagaries. AFRICON2013. IEEE2013:133-180.

Barnett WT (1972). Multipath propagation at 4, 6, and 11GHz. The Bell Syst. Technol. J. 51(2):311-361.

Barrios A (1992). Parabolic equation modelling in horizontally inhomogeneous environments. IEEE Trans. Antennas Propagat. 40(7):791-797.

Falodun SE, Okeke PN (2013). Radiowave propagation measurements in Nigeria (preliminary reports). Theor. Appl. Climatol. 113:127–135. DOI 10.1007/s00704-012-0766-z.

Freeman RL (2007). Radio system design for telecommunication, Wiley Series in Telecomm. and Signal Processing. Wiley Interscience. John Willey and Sons, Inc.

Grabner M, Kvicera V, Pechac P (2011). First and second order statistics of clear-air attenuation on 11GHz terrestrial path. 6th European conference on antennas and propagation (EUCAP). IEEE: pp. 2401-2404.

Grabner M, Kvicera V, Pechac P, Jicha O (2012). Vertical dependence of refractive Index structure constant inlLowest troposphere. IEEE Antennas Wireless Propagat. Lett. 10:1473.

Grabner M, Kvicera V, Pechac P, Valtr P, Jicha O (2013). Atmospheric refractivity profiles and microwave propagation on a terrestrial path – experiment and simulation. 13th Conference on Microwave Techniques COMITE 2013, April 17-18, Pardubice, Czech Republic.

International Telecommunication Union (ITU-R, 2001). Propagation data and prediction methods required for the design of terrestrial line of sight systems. ITU, Geneva. pp. 530-539.

International Telecommunication Union (ITU-R, 2003). Propagation data and prediction methods required for the design of terrestrial line of sight systems. ITU, Geneva. pp. 530-538.

Morita K (1970). Prediction of Rayleigh fading occurrence probability of line of sight microwave links. Rev. Elec. Comm. Lab.18:310-321.

Olsen RL, Tjelta T, Martins L, Segal B (2003). Worldwide techniques for fading distribution on terrestrial L.O.S Links: Comparison with regional techniques. IEEE Trans. Antennas Propagation. 51(1):23-30.

Seybold JS (2007). Introduction to RF propagation. Wiley Interscience. John Willey and Sons, Inc.: pp. 116-118.

Westwater ER, Snider JB, Falls MJ (1990). Ground-based radiometric observations of atmospheric emission and attenuation at 20.6, 31.65, and 90.0GHz: A comparison of measurements and theory. IEEE trans. Antennas propagation. 38(10):1569-1579.

Oyedum OD (2007). Effects of tropospheric conditions on microwave propagation in Nigeria. Nig. J. Space Res. (NJSR). 3:81-100.

Xiaohai C, Crowley TP (2011). Comparison of experimental techniques for evaluating the correction factor of a rectangular waveguide microcalorimeter. IEEE Trans. Instrum. Meas. 60(7):2690-2695.

International Journal of Physical Sciences

Related Journals Published by Academic Journals

- *African Journal of Pure and Applied Chemistry*
- *Journal of Internet and Information Systems*
- *Journal of Geology and Mining Research*
- *Journal of Oceanography and Marine Science*
- *Journal of Environmental Chemistry and Ecotoxicology*
- *Journal of Petroleum Technology and Alternative Fuels*

academicJournals